SPATIAL REGISTRATION OF TIROS-N WEATHER SATELLITE DATA

THESIS

Charles H. Larcomb
Captain, USAF

AFIT/GSO/ENS/89D-10

DEPARTMENT OF THE AIR FORCE
AIR UNIVERSITY
AIR FORCE INSTITUTE OF TECHNOLOGY

Wright-Patterson Air Force Base, Ohio

AFIT/GSO/ENS/89D-10

IMAGE NAVIGATION OF TIROS-N WEATHER SATELLITE DATA

THESIS

Presented to the Faculty of the School of Engineering
of the Air Force Institute of Technology
Air University
In Partial Fulfillment of the
Requirements for the Degree of
Master of Science in Space Operations

Charles H. Larcomb, B.A.
Captain, USAF

December 1989

Preface

Hobbyists have been receiving and displaying weather satellite images for some time. With relatively simple and inexpensive ground stations, enthusiasts can receive Automatic Picture Transmissions (APT) from both the U.S. TIROS-N satellites and the Soviet Meteor satellites. The TIROS-N polar-orbiting satellites continuously transmit weather data as they orbit the earth every 102 minutes.

The main obstacle to using these images is a lack of geographic references. Geographic boundaries are often obscured by clouds or lack of contrast. This work is aimed at removing this obstacle, to greatly enhance the usefullness of polar-orbiting weather satellite images.

I am indebted to my thesis advisor, Dr. Thomas S. Kelso, for his guidance and inspiration through no small expense of time and personal resources. Ms. Mona Smith of NOAA/NESDIS was very helpful in obtaining the NOAA publications used in this work. Finally, I thank my wife, Cirela, for her patience and support.

Charles H. Larcomb

Table of Contents

List of Figures

List of Tables

List of Symbols

Symbol	Meaning
α	convergence factor for inverse referencing algorithm
β	great circle arc from ascending node to earth location
δ	off-nadir scan angle
d	range distance from satellite to earth location
ϵ	time accuracy in calculating pixel time
ξ	oblate earth constant ($\xi = R_{eq}^2 / R_{po}^2 - 1$)
e	eccentricity of the earth meridian ellipse
Φ_{gc}, Φ_{gd}	geocentric and geodetic latitude, respectively
γ	apparent scan skew angle
GHA	Greenwich hour angle
G_0	GHA at the beginning of the year
G_1	daily increase in GHA
h	satellite height above the earth's surface
$\underline{h}$	orbit momentum vector ($\underline{r} \times \underline{v}$)
IFOV	instantaneous field of view
i, i'	orbit inclination and latitude crossing angle, respectively

Symbol	Meaning
j	angle between the equator and the great circle through ascending node and earth location
λ_{gc}, λ_{gd}	geocentric and geodetic longitude, respecively (same)
λ'	static longitude, measured from the ascending node
L	longitude distance spanned by sensor swath
l, p	line and pixel coordinates, respectively
l_0 , p_0	reference line and pixel coordinates
μ	earth gravitational constant
Ω	earth rotation rate
$\dot{\Lambda}$	orbital precession rate
P	orbital period
$\underline{r}$	satellite radius vector
$\underline{R}$	earth position vector
R_{eq}, R_{po}	earth equatorial and polar radius, respectively
$\underline{s}$	sensor scan vector ($\underline{r}$ x $\underline{v}$)
STEP	mirror step angle
θ	angular distance from the ascending node to the satellite subpoint
$\dot{\theta}$	satellite angular velocity
t	time
t_0	reference time of pixel (l_0 ,p_0)
$t_{1/2}$	time duration of half a scan line
T_l , T_p	HRPT line and pixel period, respectively

Symbo	Meaning
Ψ	earth center angle (ECA) between earth location and satellite subpoint
$\underline{v}$	satellite velocity vector
$\underline{v}_c$	satellite circular velocity vector
Z	satellite zenith angle at earth location

List of Equations

$$\tan\gamma = \tan\Psi/\sin(\Delta\theta) \quad (1)$$

$$R_E^{\,2} = d^2 + r^2 - 2dr\cos\delta \quad (2)$$

$$d = r\cos\delta - (R_E^{\,2} - r^2 \sin^2\delta)^{1/2} \quad (3)$$

$$Z = \delta + \Psi \quad (4)$$

$$\sin Z = (r/R_E)\sin\delta \quad (5)$$

$$\sin(\delta + \Psi) = (r/R_E)\sin\delta \quad (6)$$

$$\tan\delta = \sin\Psi/[(r/R_E) - \cos\Psi)] \quad (7)$$

$$d = r\cos\delta - R_E\cos(\delta + \Psi) \quad (8)$$

$$\sin\Phi_{S'} = \sin\theta \sin(i) \quad (9)$$

$$\sin\lambda'_{S'} = \cos\theta/\cos\Phi \quad (10)$$

$$\cos(i') = \sin\lambda'/\sin\theta \quad (11)$$

$$\sin(L/2) = \sin\Psi_{max}/\sin(i') \quad (12)$$

$$\Delta\lambda = L/\cos\Phi \quad (13)$$

$$(\text{passes/day}) = (\text{orbits/day})\Delta\lambda/180 \quad (14)$$

$$IFOV_{APT} = (n - 1)STEP + IFOV_{HRPT} \quad (15)$$

$$\underline{R} = \underline{r} + \underline{d} \quad (16)$$

$$\underline{s} = \underline{r} \times \underline{v} \quad (17)$$

$$\hat{\underline{d}} = -\hat{\underline{r}}\cos\delta + \hat{\underline{s}}\sin\delta \quad (18)$$

$$d = r\cos\delta - (R^2 - r^2\sin^2\delta)^{1/2} \quad (19)$$

$$\underline{d} = -\hat{\underline{r}}\{\cos\delta[r\cos\delta - (R^2 - r^2\sin^2\delta)^{1/2}]\} + \hat{\underline{s}}\{\sin\delta[r\cos\delta - (R^2 - r^2\sin^2\delta)^{1/2}]\} \quad (20)$$

$$(R_X^{\,2} + R_Y^{\,2})/R_{eq}^{\,2} + R_Z^{\,2}/R_{po}^{\,2} = 1 \quad (21)$$

$$R^2 = R_{eq}^{\,2} - \xi R_Z^{\,2} \quad (22)$$

$$\xi = R_{eq}^2 / R_{po}^2 - 1 \tag{23}$$

$$R^2 = R_{eq}^2 - \xi(r_Z + d\hat{d}_Z)^2 \tag{24}$$

$$R^2 = r^2 + d^2 - 2rd\cos\delta \tag{25}$$

$$d^2(1 + \xi\hat{d}_Z^2) - 2d(r\cos\delta - \xi r_Z\hat{d}_Z) = R_{eq}^2 - r^2 - \xi r_Z^2 \tag{26}$$

$$d = r\cos\delta - \xi r_Z\hat{d}_Z/(1 + \xi\hat{d}_Z^2) - \{[R_{eq}^2 - r^2 - \xi r_Z^2 + (r\cos\delta - \xi r_Z\hat{d}_Z)^2]/(1 + \xi\hat{d}_Z^2)\}^{1/2} \tag{27}$$

$$v_C = (\mu/r)^{1/2} \tag{28}$$

$$\dot{\theta} = (\mu/r^3)^{1/2} \tag{29}$$

$$\dot{\theta} = 2\pi/P \tag{30}$$

$$\underline{v}_C = (-\underline{\hat{r}} \times \underline{\hat{h}})v_C \tag{31}$$

$$\underline{r}(t + \Delta t) = \underline{r}(t)[\cos(\dot{\theta}\Delta t)] + \underline{v}_C(t)[\sin(\dot{\theta}\Delta t)/\dot{\theta}] \tag{32}$$

$$\underline{v}_C(t + \delta t) = -\underline{\hat{r}}(t)\{[v_C(t)/r]\sin(\dot{\theta}\Delta t)\} + \underline{v}_C(t)[\cos(\dot{\theta}\Delta t)] \tag{33}$$

$$\sin\theta_{S'} = \sin\Phi_{S'}/\sin(i) \tag{34}$$

$$t_N = t_{S'} - \theta_{S'}/\dot{\theta} \tag{35}$$

$$\cos(\lambda'_{S'}) = \cos\theta_{S'}/\cos\Phi_{S'} \tag{36}$$

$$\lambda_N = \lambda_{S'} + \lambda'_{S'} - (t_{S'} - t_N)(\Omega - \dot{\Lambda}) \tag{37}$$

$$\lambda'_E = \lambda_E - \lambda_N + (t_E - t_N)(\Omega - \dot{\Lambda}) \tag{38}$$

$$\cos\beta = \cos\Phi_E \cos\lambda'_E \tag{39}$$

$$\sin(j) = \sin\Phi_E / \sin\beta \tag{40}$$

$$\sin\Psi = \sin(j-i)\sin\beta \tag{41}$$

$$\cos\theta_{S''} = \cos\beta/\cos\Psi \tag{42}$$

$$t_{S''} = t_N + \theta_{S''}/\dot{\theta} \tag{43}$$

$$t' = t_E + \alpha(t_{S''} - t_E) \tag{44}$$

$$\alpha = 1 + \cos(i)\cos\Phi_E\,(\Omega - \dot{\Lambda})/\dot{\theta} \tag{45}$$

$$\delta_p = \mathrm{STEP}(p - 1023.5) \tag{46}$$

$$t_{l,p} = t_0 + T_l\,(l - l_0) + T_p\,(p - p_0) \tag{47}$$

$$p = 1023.5 + \delta/\mathrm{STEP} \tag{48}$$

$$l = l_0 + [t - t_0 - T_p\,(p - p_0)]/T_l \tag{49}$$

$$\tan\Phi_{gc} = [R_Z\,/(R_X^2 + R_Y^2)^{1/2}] \tag{50}$$

$$\tan[\lambda_{gc} + \mathrm{GHA}(t)] = \tan(R_Y\,/R_X) \tag{51}$$

$$\mathrm{GHA}(t) = G_0 + G_1\,t_d + \Omega t_h \tag{52}$$

$$\tan\Phi_{gd} = (R_{eq}/R_{po})^2\,\tan\Phi_{gc} \tag{53}$$

$$\lambda_{gd} = \lambda_{gc} \tag{54}$$

Abstract

The purpose of this study was to develop an algorithm to perform spatial registration of (assign geographic coordinates to) TIROS-N weather satellite data using a personal computer. Specific objectives were (1) to gather currently available information into a unified and understandable form, (2) to develop the background and related theory necessary for the registration of both High Resolution Picture Transmission (HRPT) and Automatic Picture Transmission (APT) data, and (3) to present a specific registration algorithm for TIROS-N weather satellite data.

The approach chosen is to use a general elliptical orbit model in conjunction with accurate satellite element sets (orbital parameters) to calculate accurate satellite positions at a given time. Knowing the earth movement and sensor operation as functions of time, the geographic locations of each pixel (picture element) are determined through geometric relations.

The algorithm presented converts pixel coordinates to, geographic coordinates (direct referencing) and vice versa (inverse referencing). These algorithms assume an elliptical orbit (with perturbations) and an oblate spheroid earth.

The most critical factor is found to be timing. A timing error of one second in computing satellite position produces an earth location error of about 6.5 kilometers at the satellite subpoint. A timing correction method is outlined to visually improve the image registration.

SPATIAL REGISTRATION OF TIROS-N WEATHER SATELLITE DATA

I. Introduction

Background

The TIROS-N satellite series is the set of polar orbiting satellites operated by the National Oceanographic and Atmospheric Administration (NOAA) that provides advanced environmental (weather) data. The active satellites continuously transmit both High Resolution Picture Transmission (HRPT) data (1.1 km resolution) and Automatic Picture Transmission (APT) data (4 km resolution) as they orbit the earth at an altitude of about 850 kilometers [1:2-1,3-5].

The images do not contain geographic grids or map outlines as provided by the more sophisticated high-altitude Geosynchronous Operational Environmental Satellites (GOES). These enhancements must be added manually after image reception. This spatial registration (process of assigning geographic coordinates to the satellite data) is essential to provide accurate and detailed weather information.

The HRPT signal has a high data rate and frequency. Its reception requires a fairly sophisticated ground station

using mainframe computers which also allow partial automation of the registration process. Current HRPT ground stations are expensive, costing $150,000 or more [17:2-2].

The APT signal has a low data rate and frequency permitting reception with relatively simple and inexpensive receivers [1:55]. A complete ground station can be constructed for less than $500 [17:4-1]. These, however, generally provide film or paper copies which must be registered by hand using tedious and inaccurate methods.

With the growing popularity of personal computers, computer display systems are becoming a common method of displaying weather satellite images [17:9-4]. For a modest cost, an analog-to-digital converter allows PCs to process and store APT satellite image data. Commercially available software is expensive, though, and spatial registration is still a problem.

Due to these difficulties, the usefulness of TIROS-N weather data has been largely unexploited. Most weather agencies depend heavily on data from a few costly GOES satellites of which only one is currently operating. TIROS-N data with spatial registration could provide an essential and capable backup capability, as well as coverage of polar regions. Simple, mobile APT receivers could also be easily transported to any point on the globe.

Problem Statement

The purpose of this research is to develop an algorithm to register TIROS-N weather satellite data on a personal computer. After the analog (continuous) APT data from the satellite is reconverted to digital form, the algorithm will assign geographic coordinates to each pixel (individual data element) or find the pixel corresponding to a given geographic location. This registration allows the user to add latitude/longitude grids and map overlays, display, process, analyze, and store the satellite images on a personal computer.

Objectives

This research was directed to meet the following objectives:

1. Gather currently available information necessary for HRPT and APT data registration into an accessible, unified, and understandable form
2. Develop the background and related theory for the spatial registration and use of both HRPT and APT data; and
3. Present a specific registration algorithm for TIROS-N weather satellite data

II. Literature Review

Introduction

As one author recently observed [6:898], "there are few published articles on the image referencing and geometric correction of AVHRR data." A current literature search confirmed this deficit and uncovered no articles on the registration of APT data.

Nevertheless, the basic principles that apply to spatial registration are well known. The methods used for the higher resolution HRPT data should also apply in large part to APT data.

The following paragraphs review literature on the topics pertaining to this investigation. These topics are spacecraft and sensor characteristics, satellite orbits, geometric corrections, HRPT registration methods, and AVHRR data applications.

Spacecraft and Sensor Characteristics

The TIROS-N series currently consists of two operational satellites in sun-synchronous polar orbits [8:1-7]. Detailed spacecraft and sensor characteristics are presented in the NOAA User's Guides [1; 8]. These include orbital characteristics, specific parameters on spacecraft instru-

ments, and the formats of archive data (stored data available from NOAA upon request).

The heart of the TIROS-N series spacecraft sensors is the Advanced Very High Resolution Radiometer (AVHRR). This instrument provides real-time visible and infrared data worldwide in two formats: Automatic Picture Transmission (APT) with 4 km resolution, and High Resolution Picture Transmission (HRPT) with 1.1 km resolution [1:2-1].

NOAA Technical Memorandum NESS 95 [15] provides detailed information on the operation of the AVHRR and other sensors and satellite systems. The format and parameters for both HRPT and APT data transmissions is also included. TM 95 was the major source of background information presented in this work.

NOAA Technical Memorandum NESS 107 - Rev 1 [10] provides information useful for the calibration (assigning more accurate absolute measurement values) of TIROS-N sensor data. Also, Appendix C outlines a generic registration algorithm for polar-orbiting satellites.

Satellite Orbits

Ideally, a satellite in a circular orbit about the earth follows a perfect circle determined by the laws of orbital mechanics for two-body motion. In reality, however, there are deviations due to a slight eccentricity of the satellite orbit, and differential gravity effects caused by

the sun and moon, and an earth that bulges at the equator. Measuring the exact time is also critical for accurate position determination.

Two approaches have been used to tackle these problems. One [6:898; 11:13] assumes an ideal circular orbit. Corrections are then made based on known deviations such as orbit eccentricity, or using known image features.

An alternate method is to use the actual orbital parameters in conjunction with precise time marks included in the data transmissions [18:1258]. This method yields higher accuracy than the former, but requires timely and accurate measurements of the satellite orbital parameters. This is the approach used in this work.

Geometric Corrections

Once the spacecraft position, sensor attitude, and earth position are known at a given time, the relation between an observed image point and its corresponding point on the earth's surface is a matter of geometry. This geometry includes distortions, however, which must be corrected to accurately display satellite images. The distortions due to a rotating earth and moving satellite during an image scan are relatively straightforward. The view of the earth's surface from an angle is more complicated, since the earth is not a perfect sphere. Because the satellite is in low orbit (about 850 km) with a wide field of view ($\pm$ 55.4

degrees), this skewed view of the earth causes the greatest distortions. [18:1257].

There are two conventional distortion correction methods. One is to use a spherical model of the earth and make corrections for local deviations. This method yields errors of several pixels and runs slowly. An alternate method uses known image reference points called Ground Control Points (GCPs). While very precise, this method depends on having a number of clear and identifiable GCPs in the image [18:1257]. This method may be better for registration verification.

Sun [18:1257] proposes an improved method based on an elliptical model. Computations with this method are four times faster than the spherical model with corrections, and have less than three pixel errors [18:1257].

The approach taken in this work is to provide an accurate image registration based on a general elliptical satellite orbit model and an oblate spheroid earth model. By accurately determining the geographic location of each pixel, images can be displayed without distortion in any format desired.

HRPT Registration Methods

A few authors propose specific methods for registering AVHRR HRPT data. Popta [11] uses a method to superimpose geographic data (latitude/longitude crosses and map out-

lines) on HRPT images in real-time. The model used assumes a circular orbit about a spherical earth, with corrections to account for a rotating, oblate earth, and variable satellite speed, eccentricity, equator crossing time, and nodal period. Errors of 10 km at subpoint, and up to 21 km at edges are noted, due to "low accuracy" orbital data [11:20-21].

This method is near real-time (5 minutes run time before data receipt), but has several disadvantages. Since the orbital track is different for each pass, images cannot be compared directly in sequence for time-series analysis. This method does not use the accurate time marks present in the data. Also, geographic coordinates are only assigned to image locations where the grid lies, not to all image locations [11:1,3,9].

Tozawa presents another registration approach. Here, AVHRR data is mapped to a surface coordinate system using a mapping function. This function, solved by approximation, is based on current satellite orbit parameters provided by NOAA. GCPs are not used in this method because the mapping function is very complex over the 3000 km image swath. Also, few GCPs can be found in ocean areas.

The author claims the procedure is fast and accurate. However, he uses one GCP to adjust the data presented, citing inaccurate orbital data [19:46,51].

Ho [6] provides a better method. A corrected, spherical model and a spherical satellite orbit are used. Nodal information and the time of first scan line are included. The apparent satellite height and inclination are adjusted using one GCP. Finally, the resulting registration is verified using 11-25 GCPs for reference. Average errors are 8 pixels without the GCP, and 3 pixels with it [6:898-900].

The error rate with one GCP is excellent. A disadvantage for real-time processing is that the operator has to interrupt the registration to locate a GCP. While the author asserts that GCP location can be automated, no method is suggested.

An excellent registration method is presented by Sun [18] using a two-step approach. First, an ellipsoidal model of the earth provides corrections for the entire image. The time code imbedded in each scan line is used to determine the satellite position. Second, a template matching using 6-10 GCPs corrects residual distortions in a local area of interest.

The first step reduces errors to 0-3 pixels and works four times faster than a spherical model with corrections. If greater accuracy is desired, the second step removes virtually all geometric distortions [18:1257].

Sun also employs an interesting time reduction technique to process over 2048x4500 pixels present in each image.

4x17 pixel blocks are processed by performing calculations for the center point and using bilinear interpolation for the remaining points in the block. While not an objective of this thesis, this method could be applied to reduce computer processing time.

Emery [3] provides a good summary and review of current AVHRR registration techniques. A sample application using HRPT data compares their relative performance.

AVHRR Data Applications

Besides the obvious use of AVHRR data for routine weather observation and forecasts, there are other useful applications. Compared to LANDSAT images AVHRR data has significant advantages, despite the reduced resolution [5; 9]. AVHRR images are available 2-4 times each day, compared to once every 18 days (at best) for LANDSAT. The field of view is much wider for AVHRR, providing greater coverage [5:63-65]. These advantages proved to be an attractive tool for agricultural monitoring over France [7:1041] and observation of sea surface temperatures near Japan [9:1259].

While APT data has lower resolution than HRPT data, it could prove to be very useful because of its widespread availability. Unlike HRPT, receipt of APT is not limited to a few expensive ground receiving stations.

The approach of this research is to use accurate position calculations with precise time code information for

image registration. This should allow fully automated operation and still provide an accurate registration.

Summary

The basic principles involved in image registration are well known. While no application has been made to APT data, a few methods have been developed for HRPT data. Due to the data similarities, these provide an excellent approach for APT data.

The problem presented involves a trade-off between processing time and registration accuracy. Sun presents an excellent two-step method which seems to optimize this trade-off, at least for HRPT data.

The two basic registration methods are to use an accurate orbital prediction model, or to manually identify known GCP earth locations. The approach used here is a general elliptical orbit model (with perturbations), an oblate spheroid earth model, and accurate time code information.

AVHRR data has important applications in addition to weather monitoring. The development of a registration algorithm for both HRPT and APT data will make TIROS-N weather data even more useful and accessible.

III. Development

Introduction

The earth data viewed by the satellite consists of a series of individual picture elements (pixels). Like tiles on a mosaic, these form an image of the earth scene as the satellite sensor scans the area.

The location on the earth's surface viewed in each pixel is determined by (1) the satellite position and orientation in space (2) the sensor operation, and (3) the earth's orientation in space. All three vary in time. Through geometric relations, each pixel's location is determined by its time of observation.

To understand these relations, a general examination of the earth, satellite, and sensor characteristics is first presented. Second, the format and nature of the pixel data is examined. Third the relation between each pixel element and its corresponding earth location is derived. Finally, an algorithm is presented to convert pixel coordinates to geographic coordinates and vice versa.

Earth Characteristics

To a first approximation, the earth is spherical with the same volume as a sphere with a radius of 6371 km [4:797]. Any location on the surface of the earth can be

referenced by geocentric latitude and longitude coordinates with respect to the earth's center and equatorial plane.

The earth rotates from west to east about its north-south axis as it orbits the sun. During one tropical year (365.2422 days), the earth makes one extra revolution of 360 degrees relative to the stars (366.2422 revolutions in all). The mean rate of revolution is 360.9856 deg/day (15.0411 deg/hr or 0.2507 deg/min) [20:B6]. Viewed from a fixed location and direction in space, each earth location will move from west to east at 15.0411 deg longitude/day along its parallel of latitude (nearly constant).

Actually, the earth bulges at the equator and sags at the poles due to the rotational forces. Its shape is better modeled as an oblate spheroid whose radius is a function of latitude. In the International Astronomical Union model (IAU; 1976), the mean equatorial and polar radii are 6378.140 km and 6356.755 km, respectively [20:K13]. This represents an eccentricity of 0.08182. At NOAA, radii values of 6378.144 km and 6356.759 km are used [10:C-10].

Even the ellipsoid model is an approximation. The equator is slightly elliptical with an eccentricity of about 1×10^{-5} [12:25]. This, combined with irregularities in the earth's crust, cause the local acceleration of gravity to vary [12:38]. The net effect is to produce small changes in the satellite motion and viewing geometry.

Satellite Orbits

The TIROS-N series of satellites are in polar orbits, crossing the equator twice and passing over both polar regions once on each orbit. The rotation of the earth under the satellite causes the suborbital track to shift westward.

The gravitational attraction of the earth's equatorial bulge causes the line of nodes of the orbital plane to precess eastward (rotate about the earth's axis). For sun-synchronous satellites, the orbital inclinations are chosen to make the rate of precession equal to the change in orientation with respect to the sun as the earth proceeds in its orbit about the sun. On average, this rate is 0.9856474 deg/day (east longitude) [20:B6]. The TIROS-N satellites are sun-synchronous, passing over a given earth location at about the same local time every day.

The designed TIROS-N constellation consists of two satellites in sun-synchronous orbits. The nominal orbital parameters of height, inclination, period, and increment (longitude shift between successive orbits) are summarized in Table 1.

The two circular orbits intersect at right angles, so that one satellite follows the other about six hours later. The orbits are chosen to have a morning satellite that passes overhead on a descending pass between 0600 and 1000

Table 1. TIROS-N Nominal Orbital Parameters [1:3-5]

Height (km)	Inclination (deg)	Period (min)	Increment (deg W)	Orbits (#/day)
833	98.739	101.38	25.40	14.18
870	98.899	102.37	25.59	14.07

local mean solar time (LMT), and an afternoon satellite that passes overhead on an ascending pass between 1400 and 1800 LMT (see Figure 1) [1:3-6].

New satellites are put into orbit to replace aging ones in order to maintain the constellation. The replaced satellites may continue to transmit data as long as operational.

As of this writing, NOAA-10 and NOAA-11 are the primary satellites of the TIROS-N constellation. NOAA-9 continues to transmit when not in conflict with NOAA-11. A sample of orbital data is given in Table 2.

Orbital data may be obtained from the NOAA Direct Readout Users Electronic Bulletin Board (EBB) [17:7-3] or the TBUS-1 and TBUS-2 bulletins transmitted through the National Weather Service Communications Center (KWBC) [1:5-2].

Small departures from circular sun-synchronous orbits occur due to initial orbit injection errors and subsequent perturbations. Initial orbital parameters are expected to meet the target values within the following limits [15:21]:

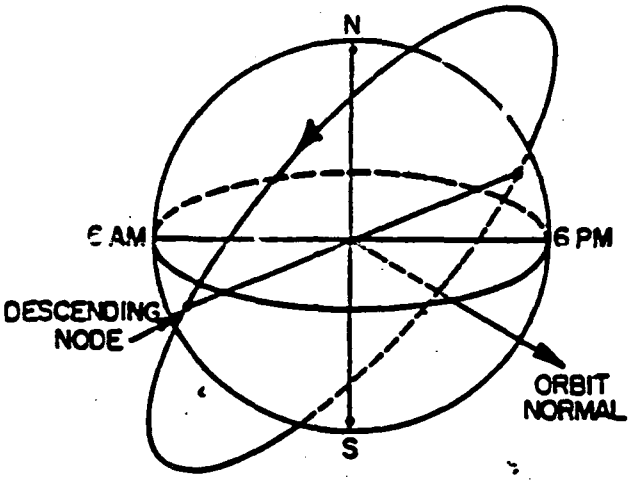

AM DESCENDING NODE ORBIT

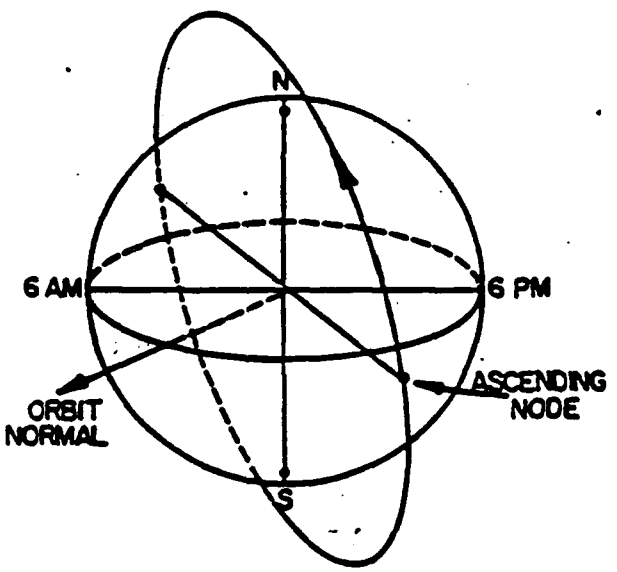

PM ASCENDING NODE ORBIT

Figure 1. TIROS-N Constellation Orbits [1:3-7]

Table 2. Sample Orbital Prediction Data [16]

Orbital Prediction Data for August 1989

	NOAA-9	NOAA-10	NOAA-11
Orbit Number	23879	14906	4380
Equator Crossing Time (Z)	0123.45	0016.35	0023.89
Long. Ascending Node (deg)	129.61W	71.03W	158.76W
Nodal Period (minutes)	102.0426	101.2340	102.1064
Frequency (MHz)	137.62	137.50	137.62
Increment (deg)	25.51	25.31	25.53

Altitude (average) : ± 15 km
Inclination : ± 0.150 deg
Apogee/Perigee Difference : less than 56 km

Dominant perturbations include the gravitational attraction of the sun and moon, drag, and the varying gravity of an irregular earth.

The spacecraft's attitude is controlled by the Attitude Determination and Control System (ADACS). The ADACS uses three orthogonal Reaction Wheel Assemblies (RWA) in combination with earth and sun sensors to maintain a fixed orientation with respect to local nadir (straight down from the satellite towards the center of the earth). This orientation is maintained within 0.2 degrees.

Departure from ideal circular orbits, combined with local perturbations, produce small attitude errors. Analys-

is has shown that attitude is generally maintained within 0.12 degrees, with only brief perturbations of up to 0.2 degrees [15:5]. Assuming a spherical earth with radius of 6371 km, these correspond to horizontal deviations at the subpoint of 1.74-2.91 km and 1.82-3.04 km at the nominal satellite altitudes of 833 km and 870 km, respectively.

Sensor Characteristics

The current TIROS-N spacecraft, called Advanced TIROS-N (ATN), carry several sensor systems including the following: TIROS Operational Vertical Sounder (TOVS), consisting of the High Resolution Infrared Radiation Sounder (HIRS/2), Stratospheric Sounding Unit (SSU), and Microwave Sounding Unit (MSU); Advanced Very High Resolution Radiometer (AVHRR); Space Environmental Monitor (SEM); Data Collection System (DCS); and Search and Rescue System (SAR) [13:2-3]. Table 3 summarizes their functions.

The earth images are derived from the AVHRR sensor. This is the primary data source for both High-Resolution Picture Transmission (HRPT) at full resolution, and Automatic Picture Transmission (APT) at reduced resolution.

The AVHRR is a scanning radiometer, measuring radiant energy in four (AVHRR/1) or five (AVHRR/2) spectral channels (see Table 4) [15:44]. NOAA-10 carries the last four-channel AVHRR, while NOAA-9 and NOAA-11 have five-channel AVHRR [8:1-34,1-40,B-3; 10:Appendix B (NOAA-F/9 and

Table 3. Advanced TIROS-N Primary Sensors [17:3-4]

1. TIROS Operational Vertical Sounder (TOVS)

   a. Measures temperature profile of earth's atmosphere from surface to 10 millibars

   b. Measures water vapor, ozone, carbon dioxide, and oxygen content of earth's atmosphere

2. Advanced Very High Resolution Radiometer (AVHRR)

   a. Measures radiation in visible and infrared spectra

   b. Primary source of data for High Resolution Picture Transmission (HRPT) and Automatic Picture Transmission (APT) data

3. Space Environment Monitor (SEM)

   Detects radiation from space at various wavelengths

4. Data Collection System (DCS)

   Collects data from earth-based environmental platforms

5. Solar Backscatter Ultraviolet Radiometer (SBUV)

   a. Measures total ozone content and vertical distribution

   b. Carried on spacecraft in afternoon ascending orbits

6. Search and Rescue (SAR)

   Detects and locates emergency beacon radio signals carried on ships and aircraft

7. Earth Radiation Budget Experiment (ERBE)

   Experiment to gather data on earth's average radiation budget

Table 4. AVHRR Spectral Channels [15:44]

AVHRR/1 (4 channels)		AVHRR/2 (5 channels)	
Channel	Wavelength (microns)	Channel	Wavelength (microns)
1	0.55 - 0.68	1	0.58 - 0.68
2	0.725 - 1.10	2	0.725 - 1.10
3	3.55 - 3.93	3	3.55 - 3.93
4	10.5 - 11.5	4	10.3 - 11.3
5	(Channel 4)	5	11.5 - 12.5

NOAA-G/10),2-Rev,3-Rev] (Note: NOAA-C/7 and NOAA-G/10 should be listed as having five- and four-channel AVHRR, respectively, as in Appendix B).

The Instantaneous Field of View (IFOV) for all channels is 1.3 mr $\pm$ 0.1 (1mr = 10^{-3} radians). The IFOV of all channels are also coincident within 0.1 mr [15:44]. This particular IFOV was chosen so that subsequent scans are contiguous at the subpoint as the satellite orbits the earth [15:43].

The AVHRR utilizes a rotating mirror to scan through 360 degrees at a rate of 360 revolutions per minute (rpm). Each scan is perpendicular to the satellite's direction of motion, crossing through the satellite subpoint (nadir)

[15:43]. The scan angle represents the mirror angle measured in reference to the nadir direction.

Thus, the AVHRR is continuously sensing radiation in all channels as the IFOV rotates through 360 degrees. Since the mirror rotates at 360 rpm, this produces 6 lines per second. The scan direction is from the space-view side of the satellite across the earth toward the sun side (from right to left) [15:46].

One scan across the earth produces a line of data referred to as a "scan line." Each scan line is skewed by the forward motion of the satellite during the scan.

The sensor actually scans along a scan vector which is perpendicular to both the satellite's position and velocity vectors. Projected onto the earth's surface, this forms a great circle arc at right angles to the satellite track (see Figure 2).

Applying the four-parts formula (cosacosC = sinacotb - sinCcotB) to Figure 2, the scan skew γ is given by

$$\tan\gamma = \tan\Psi/\sin(\Delta\theta) \qquad (1)$$

where

Ψ = earth center angle (radians)
$\Delta\theta$ = satellite angular progress (radians)

All distances along the scan line are proportional to the ECA by a factor of $\sin\gamma$. This is used in calculating the along-line resolution.

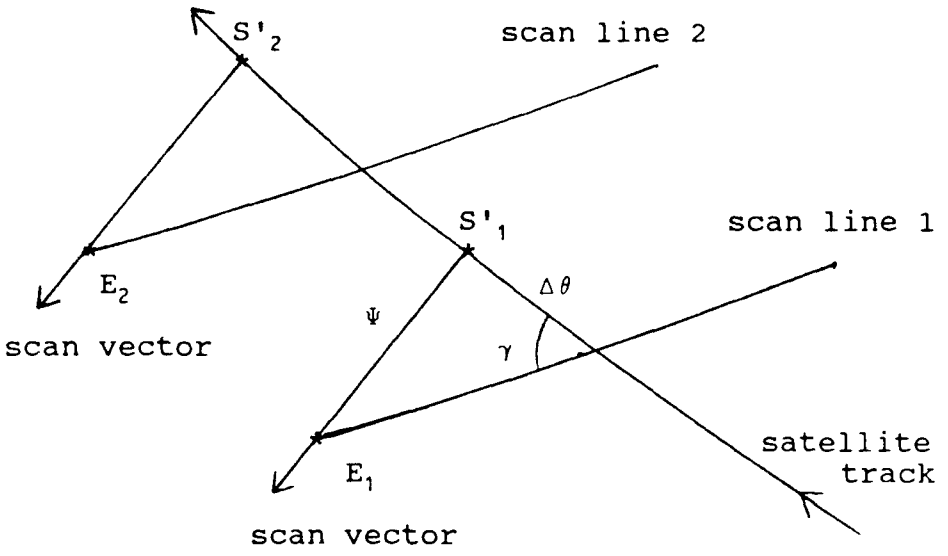

Legend

Points		Angle	
E:	Earth location	γ:	Scan skew
S':	Satellite subpoint		

Arcs

Ψ: Earth Center Angle (ECA) from S' to E
Δθ: Angular distance along satellite orbit

Figure 2. AVHRR Scan Line Skew

During half a scan line after nadir, the satellite travels an angular distance $\Delta\theta = (2\pi/P)t_{1/2}$, where P is the satellite period, and $t_{1/2}$ is the time to complete half a scan line (0.02563 seconds). The ECA is also at a maximum, Ψ_{max}. For the nominal 870 km orbit with a period of 102.37

min, Ψ_{max} = 13.86 deg (0.2420 rad) and $\Delta\theta$ = 0.001502 deg (1.5886 mr), giving a scan skew of 89.63 deg.

Some authors [3; 6] have referenced the scan angle to the satellite subpoint at the center of the scan line. Actually, the subpoint continues to move during the scan. The skewed nature of the scan line produces an apparent scan angle that has more to do with the problem of displaying the data than the actual operation of the scan mirror. In this work the scan angle is defined as the actual mirror angle measured in reference to the subpoint direction at the time of viewing.

Sensor Data

The TIROS-N data handling subsystem has two information processors: the TIROS Information Processor (TIP) for low data rates, and the Manipulated Information Rate Processor (MIRP) for high data rates. The data flow is outlined in Figure 3.

The TIP formats (and controls) the data output from the low-bit-rate instruments (HIRS/2, MSU, etc.) and the telemetry data. It also adds a time code accurate to one millisecond (see Figure 4), identification, and synchronization [15:78].

The MIRP processes and formats (and controls) data from the AVHRR, adding synchronization, telemetry, and a time

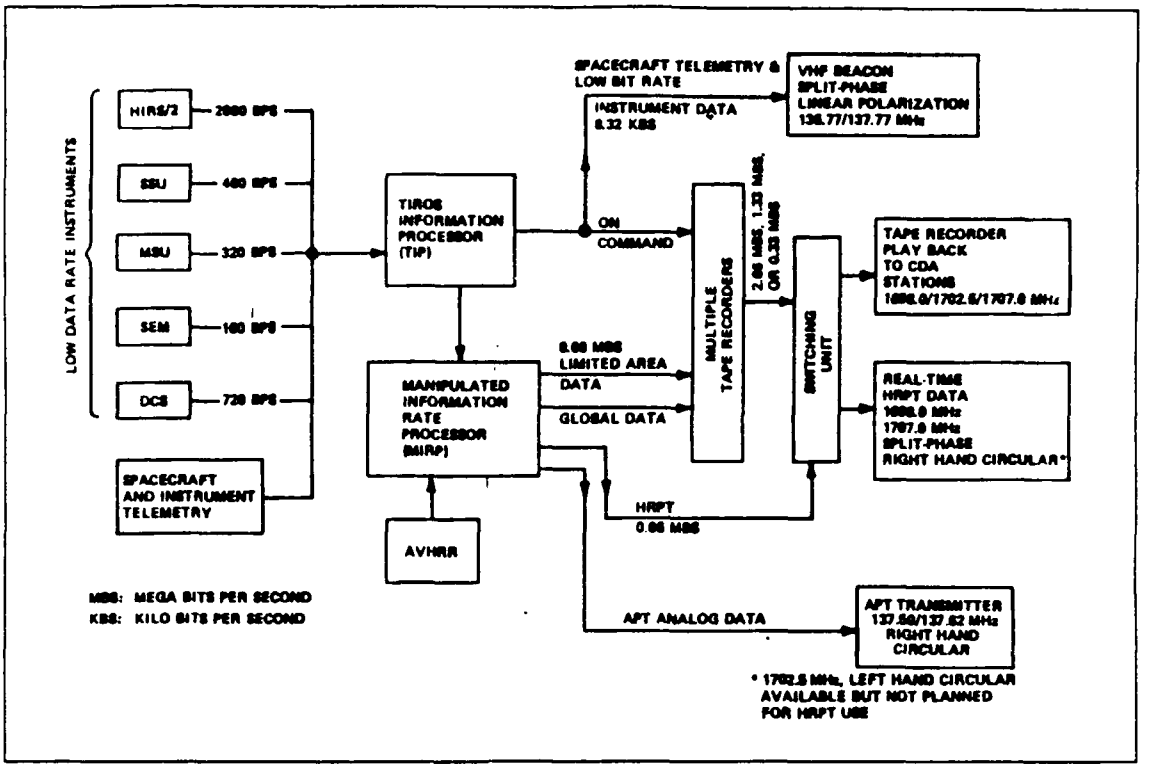

Figure 3. TIROS-N Data Flow Diagram [15:7]

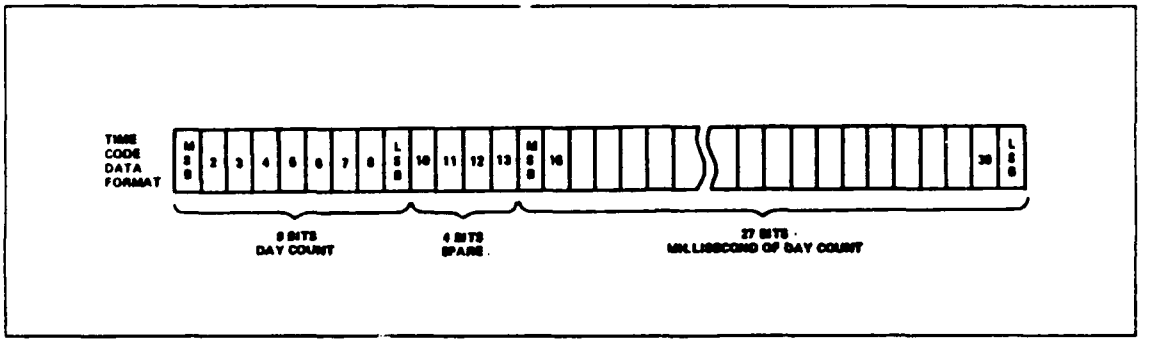

Figure 4. TIP Time Code Format [15:9]

code. TIP data is also included (except for APT processing). MIRP output is used for the following: real-time HRPT and APT transmissions, tape-recorded Global Area Cover-

age (GAC), and Local Area Coverage (LAC) [15:9-11]. Table 5 summarizes the MIRP output characteristics.

Table 5. MIRP Output Characteristics [15:11]

	HRPT/LAC	GAC	APT
Form of data	Serial digital bit stream of 10-bit words, MSB first		Analog AM on 2,400 Hz subcarrier
Line rate	6/sec	2/sec	2/sec
Word rate (words/sec)	66,540	6,654	4,160 before digital-to-analog conversion
Number of AVHRR channels	5	5	2
Words of earth data per line per channel	2048	409	909 before digital-to-analog conversion
Processing of AVHRR data	Formatting only	Resolution reduction; formatting	Resolution reduction; formatting
Other data than AVHRR	TIP; time code	TIP; time code	Minute marks Calibration wedge

When the AVHRR scan mirror reaches a predetermined pre-earth position, a synchronization pulse is generated and sent to the MIRP. This event becomes the reference for all subsequent event timing [15:12].

Event timing is based on a 0.9984 megahertz (MHz) internal clock [14]. At this frequency, the clock makes 0.9984×10^{6} counts every second, or one count every $1.001602564 \times 10^{-6}$ seconds. Events may also be referenced in Standard Time Units (STU), where 1 STU = 1000 counts. Table 6 summarizes the timing of major events.

Table 6. MIRP Event Timing [14]

Count	STU	Event
0	0	Frame sync, bit 1, word 1
8,600	8.6	First pulse of earth data
34,200	34.2	Nadir
59,775	59.775	Last pulse of earth data
68,400	68.4	End

The MIRP issues sampling commands to the AVHRR, making instantaneous measurements of the instrument readings. Each reading is coded as a ten-bit word with the most significant bit (MSB) first. In each scan, the AVHRR produces 2,048 samples of earth data for each channel, along with other reference samples as indicated in Figure 5 [15:10-13].

As illustrated in Figure 6, in each AVHRR scan line, 2047 words (2048 - 1) are produced in 51,175 time clock counts (59,775 - 8,600), or one word every 25 counts (25.04006×10^{-6} seconds). The mirror rctates at 6 rev/sec,

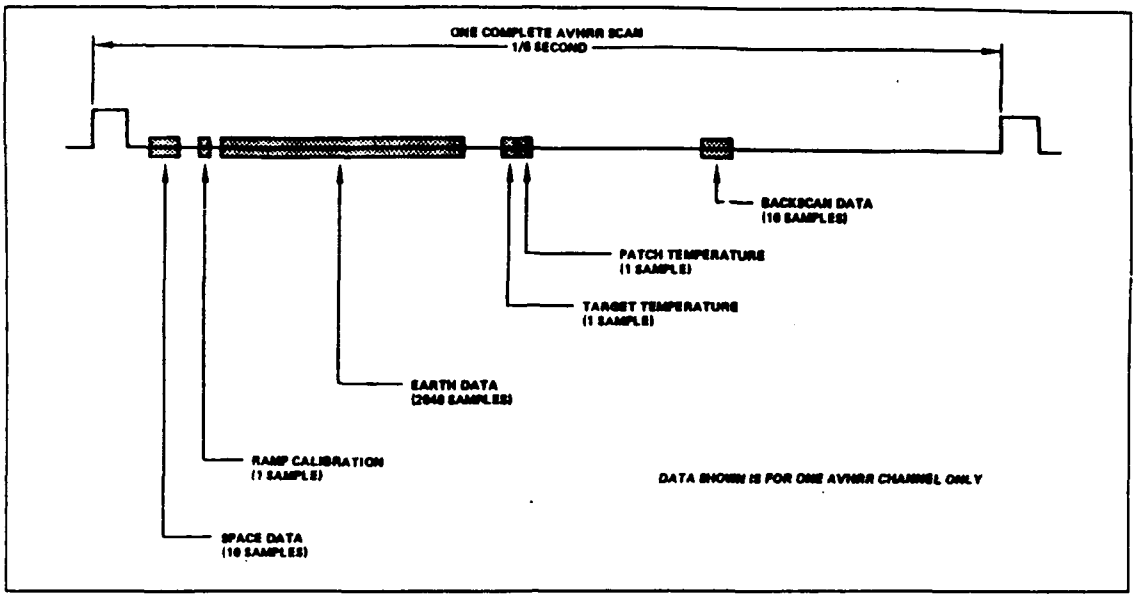

Figure 5. AVHRR Data Sampling Areas [15:13]

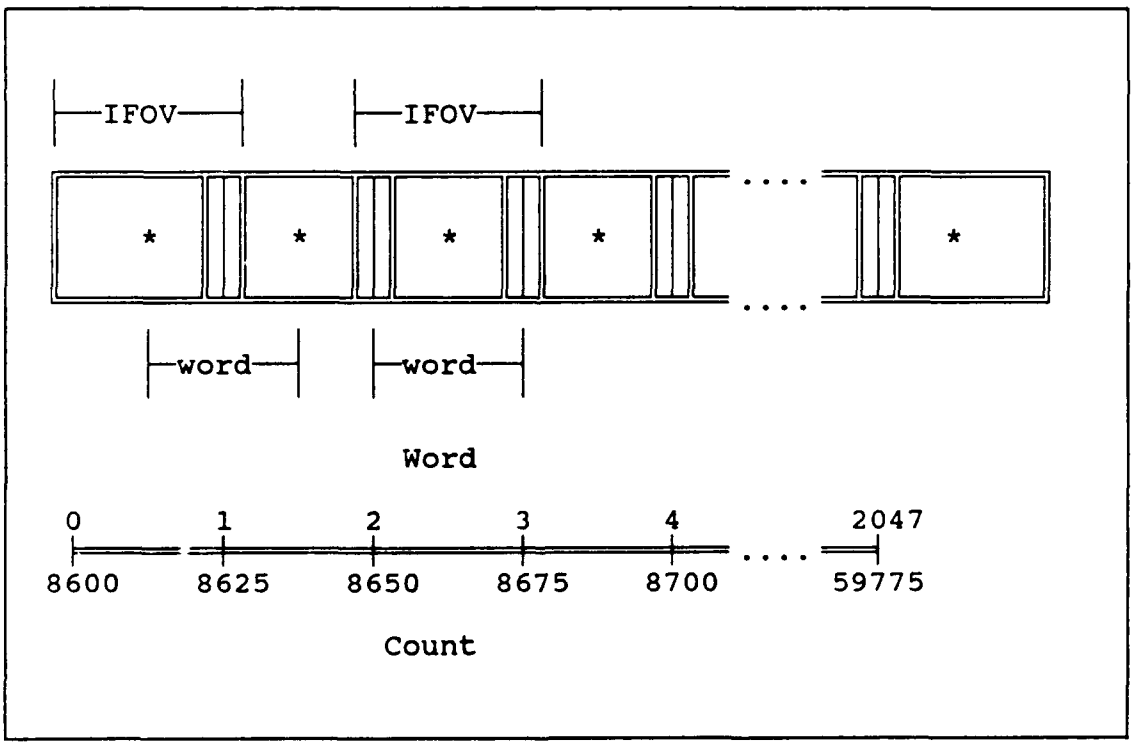

Figure 6. AVHRR Scan Line IFOV

so there are 0.9439882×10^{-3} radians (mr) per word, or 110.7692308 degrees per line of 2048 words. Since the IFOV is 1.3 mr, the views of consecutive pixels (words) overlap by about 0.36 mr (27% of the IFOV).

HRPT/APT Processing

The MIRP also performs the function of processing two channels of AVHRR data into a reduced resolution format (and lower data rate) for APT transmission. Only one AVHRR line in three is processed for each of the two APT channels, producing two lines/sec of APT data. The APT samples are then converted to an analog format with an accuracy of 8 MSBs of the original 10-bit AVHRR words [15:63]. The phasing of the MIRP output is summarized in Figure 7.

The data reduction algorithm divides each scan into five regions according to the angular distance from nadir as shown in Table 7. This algorithm reduces 2,048 HRPT words to 909 APT words per channel, providing a nearly uniform resolution of 4 km along the scan line.

The correspondence between APT and HRPT pixels is given in Table 8. The scan angle is referenced to nadir (0 deg). Pre-nadir angles are defined as negative and post-nadir angles defined as positive.

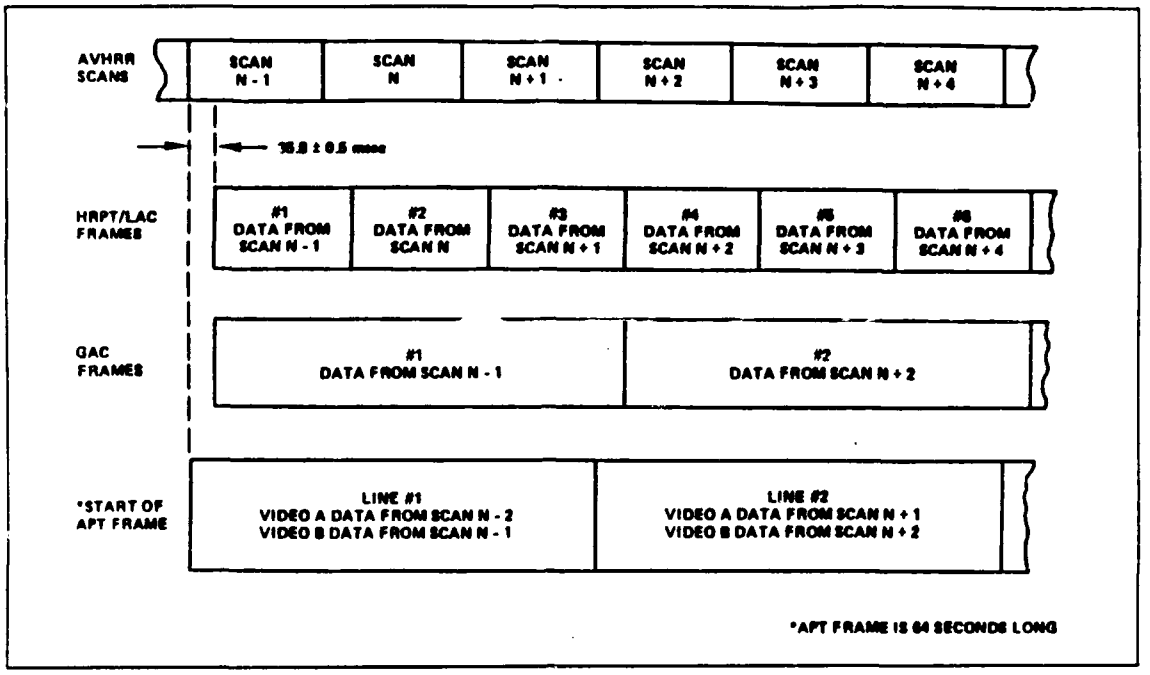

Figure 7. MIRP Output Phasing [15:14]

Table 7. HRPT/APT Data Reduction Algorithm [15:16]

Region	Scan Angle * degrees (±)	Reduction Method
1	0.0 - 16.9	Average 4 samples (contiguous)
2	16.9 - 34.8	Average 2 samples, skip 1
3	34.8 - 43.8	Average 2 samples (contiguous)
4	43.8 - 48.8	Average 1 1/2 samples (A+B)/2; (B+C)/2
5	48.8 - 55.4	Retain original (No reduction)

* Measured from nadir

Table 8. HRPT/APT Pixel Correspondence

	HRPT			APT	
Scan Angle	Words	Pixel	Ratio	Pixel	Words
-55.38 to -48.84	121	0-120	1:1	0-120	121
-48.84 to -43.81	93	121-213	3:2	121-182	62
-43.81 to -34.83	166	214-379	2:1	183-265	83
-34.83 to -16.98	330	380-709	3:1	266-375	110
-16.98 to 16.98	628	710-1337	4:1	376-532	157
16.98 to 34.83	330	1338-1667	3:1	533-642	110
34.83 to 43.81	166	1668-1833	2:1	643-725	83
43.81 to 48.84	93	1834-1926	3:2	726-787	62
48.84 to 55.38	121	1927-2047	1:1	788-908	121
Total	2048	0-2047	(4km)	0-908	909

Data Format

HRPT is a real-time, high-data-rate digital transmission (see Table 9 and Table 10). The HRPT transmission contains all spacecraft instrument data [10:10-rev]. This consists of output from the five AVHRR channels, multiplexed with the TIP output (including telemetry).

The HRPT line and minor frame formats are summarized in Figure 8 and Table 11. Three minor frames make up a major frame. The TIP data is updated only once every major frame (every three minor frames) [10:18,20-23; 15:71-75].

Table 9. HRPT Characteristics [10:13]

Line rate	6 lines/second
Carrier modulation	Digital split phase, phase modulated
Transmit frequency	1698.0 MHz or 1707.0 MHz
Transmit power	8 watts nominal
EIRP (approximate)	39.0 dBm
Polarization	Right hand circular
Spectrum bandwidth	2.4 MHz (3dB)

Table 10. HRPT Parameters [10:17]

Major Frame	Rate	2 frames/sec
	Format	3 minor frames
Minor frame	Rate	6 frames/sec
	Format	See Figure 8
	Words	11,090
Word	Rate	66,540 words/sec
	Words/channel	2,048/line
	Bits 10	
	Order	Bit 1 = MSB (Most Significant Bit) Bit 10 = LSB (Least Significant Bit)
Bit	Rate	665,400 bits/sec
	Format	Split phase

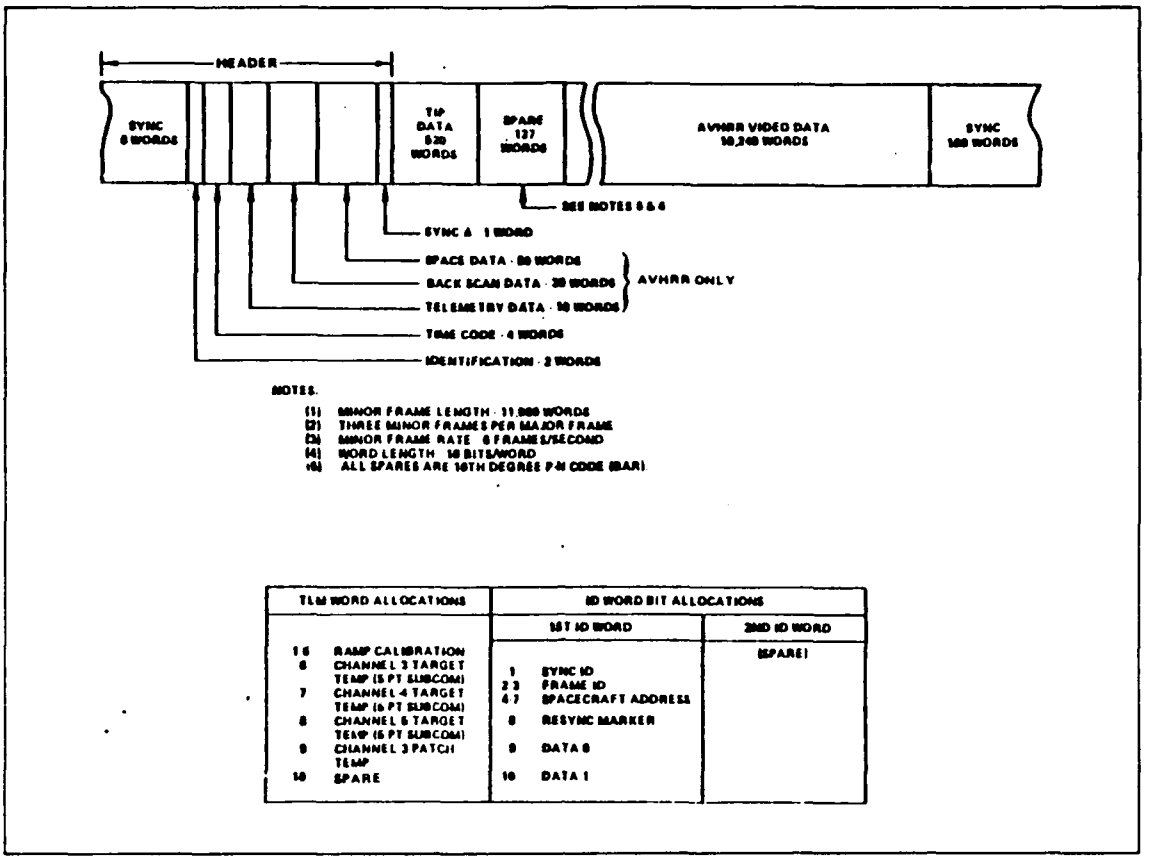

Figure 8. HRPT Line Format [10:18]

APT is a realtime, medium-data-rate analog transmission (see Table 12 and Table 13). The APT transmission concontains MIRP processed data from two ground selectable AVHRR channels, labeled channels A and B [10:10-rev].

Channels A and B are multiplexed with telemetry and space data, then converted to an analog signal which amplitude modulates (AM) a 2400 Hz subcarrier for analog transmission on a frequency modulated (FM) carrier [10:10-Rev; 15:16].

Table 11. HRPT Minor Frame Format [10:20]

	Function	No. of Words	Word Position	Bit No. 1 2 3 4 5 6 7 8 9 10 — Plus word code & meaning
HEADER	Frame sync	6	1	1 0 1 0 0 0 0 1 0 0 — First 60 bits from a 63-bit PN[1] generator started in the all 1's state. The generator polynominal is $X^6 + X^5 + X^2 + X + 1$
			2	0 1 0 1 1 0 1 1 1 1
			3	1 1 0 1 0 1 1 1 0 0
			4	0 1 1 0 0 1 1 1 0 1
			5	1 0 0 0 0 0 1 1 1 1
			6	0 0 1 0 0 1 0 1 0 1
	ID (AVHRR)	2	7	Bit 1; 0 = internal sync; 1 = AVHRR sync Bits 2 & 3; 00 = not used; 01 = minor frame 1; 10 = minor frame 2, 11 = minor frame 3 Bits 4-7; spacecraft address; bit 4 = MSB, bit 7 = LSB Bit 8; 0 = frame stable; 1 = frame resync occurred Bits 9-10; spare; bit 9 = 0, bit 10 = 1
			8	Spare word; bit symbols undefined
	Time code	4	9	Bits 1-9; binary day count; bit 1 = MSB; bit 9 = LSB Bit 10; 0; spare
			10	Bits 1-3; all 0's; spare 1, 0, 1 Bits 4-10; part of binary msec of day count; bit 4 = MSB of msec count
			11	Bit 1-10; part of binary msec of day count;
			12	Bit 1-10; remainder of binary msec of day count; bit 10 = LSB of msec count
	Telemetry (AVHRR)	10	13	Ramp calibration AVHRR channel 1
			14	Ramp calibration AVHRR channel 2
			15	Ramp calibration AVHRR channel 3
			16	Ramp calibration AVHRR channel 4

(1) PN = pseudo noise

HEADER	Telemetry (cont.) (AVHRR)	10	17	Ramp calibration AVHRR ch 5 — Each of these words is a 5-ch subcom, 4 words of IR data plus a subcom reference value
			18	AVHRR internal target[2] temperature data
			19	
			20	
			21	AVHRR patch temperature
			22	0 0 0 0 0 0 0 0 0 1 spare
	(AVHRR) Internal target data	30	23 ↓ 52	10 words of internal target data from each AVHRR ch 3, 4, and 5. These data are time multiplexed as ch 3 (word 1), ch 4 (word 1), ch 5 (word 1), ch 3 (word 2), ch 4 (word 2), ch 5 (word 2), etc.
	Space data (AVHRR)	50	53 ↓ 102	10 words of space-scan data from each AVHRR channel 1, 2, 3, 4, and 5. These data are time multiplexed as ch 1 (word 1), ch 2 (word 1), ch 3 (word 1), ch 4 (word 1), ch 5 (word 1), ch 1 (word 2), ch 2 (word 2), ch 3 (word 2), ch 4 (word 2), ch 5 (word 2), etc.
	Sync Δ (AVHRR)	1	103	Bit 1; 0 = AVHRR sync early; 1 = AVHRR sync late Bits 2-10; 9-bit binary count of 0.9984-MHz periods; bit 2 = MSB, bit 10 = LSB

(2) As measured by a platinum resistance thermometer embedded in the housing.

Table 11 (continued)

Function	No. of Words	Word Position	Bit No. 1 2 3 4 5 6 7 8 9 10 Plus Word Code & Meaning
Tip data	520	104 ⋮ 623	The 520 words contain five frames of TIP data (104 TIP data words/frame) Bits 1-8: exact format as generated by TIP Bit 9: even parity check over bits 1-8 Bit 10: - bit 1
Spare words	127	624 625 626 627 628 ⋮ 748 749 750	1 0 1 0 0 0 1 1 1 0 1 1 1 0 0 0 1 0 1 1 0 0 0 0 1 0 1 1 1 1 1 0 1 1 0 0 0 1 1 1 1 1 0 1 0 1 0 0 1 0 ⋮ 1 0 0 1 0 1 1 0 1 0 1 1 0 0 1 0 0 0 1 0 1 0 0 0 0 0 0 0 0 0 Derived by inverting the output of a 1023-bit PN sequence provided by a feedback shift register generating the polynominal: $X^{10} + X^5 + X^2 + X + 1$ The generator is started in the 1's state at the beginning of word 7 of each minor frame.
Earth data (AVHRR)	10,240	751 752 753 754 755 756 ⋮ 10,985 10,986 10,987 10,988 10,989 10,990	Ch 1 - Sample 1 Ch 2 - Sample 1 Ch 3 - Sample 1 Ch 4 - Sample 1 Ch 5 - Sample 1 Ch 1 - Sample 2 ⋮ Ch 5 - Sample 2047 Ch 1 - Sample 2048 Ch 2 - Sample 2048 Ch 3 - Sample 2048 Ch 4 - Sample 2048 Ch 5 - Sample 2048 Each minor frame contains the data obtained during one earth scan of the AVHRR sensor. The data from the five sensor channels of the AVHRR are time multiplexed as indicated
Auxiliary sync	100	10,991 10,992 10,993 10,994 ⋮ 11,089 11,090	1 1 1 1 1 0 0 0 1 0 1 1 1 1 1 1 0 0 1 1 0 1 1 0 1 1 0 1 0 1 1 0 1 0 1 1 1 1 0 1 ⋮ 0 1 1 1 1 1 0 0 0 0 1 1 1 1 0 0 1 1 0 0 Derived from the noninverted output of a 1023-bit PN sequence provided by a feedback shift register generating the polynominal: $X^{10}, X^5 + X^2, X + 1$ The generator is started in the all 1's state at the beginning of word 10,991

As of this writing, the primary spacecraft (NOAA-10 and NOAA-11) are transmitting one visible and one infrared (IR) channel during spacecraft day, and two IR channels during

Table 12. APT Characteristics [10:11]

Line rate	2 lines/sec
Data resolution	4 km (nearly uniform)
Carrier modulation	Analog
Transmit frequency	137.50 MHz or 137.62 MHz
Transmit power	6 watts nominal
Polarization	Right hand circular
Subcarrier frequency	2.4 kHz
Carrier deviation	± 17 kHz
Low pass filter (ground station)	1.4 kHz 7th-order linear recommended
Synchronization	Channel A: 7 pulses at 1040 pps with 50% duty cycle Channel B: 7 pulses at 832 pps with 60% duty cycle

spacecraft night via APT. NOAA-9 transmits one visible channel and one IR channel throughout its orbit [16].

The APT line and frame formats are summarized in Figure 9, Figure 10, and Figure 11. Note that one frame consists of 128 lines. Each APT frame contains one telemetry frame of 16 wedges repeated on 8 consecutive lines, both after channel A and after channel B data.

Minute markers are also included in four consecutive lines (two white, two black). While the time of each mark is not specified, limited observation found the start of

Table 13. APT Parameters [10:13]

Frame	Rate	1 frame per 64 seconds
	Format	128 lines
Line	Rate	2 lines/sec
	Format	See Figures 8, 9 and 10
	Words	2,080
	Channels	2 (selected)
Word	Rate	4,160 words/sec
	Words/channel	909
	Analog-to-Digital Conversion Accuracy	The 8 Most Significant Bits (MSBs) of the 10-bit AVHRR words
Low-pass filter	Type	3rd-order Butterworth-Thompson
	Bandwidth	2400 Hz (3 dB)

each minute indistinguishable from the first white line in the four-line sequence. This work assumes that the beginning of each minute coincides with the start of the synchronization pulse of channel A in each line with the first white minute marker.

To process the APT data on a digital computer, the analog APT signal received must be reconverted to digital form after demodulation. This is accomplished by sampling

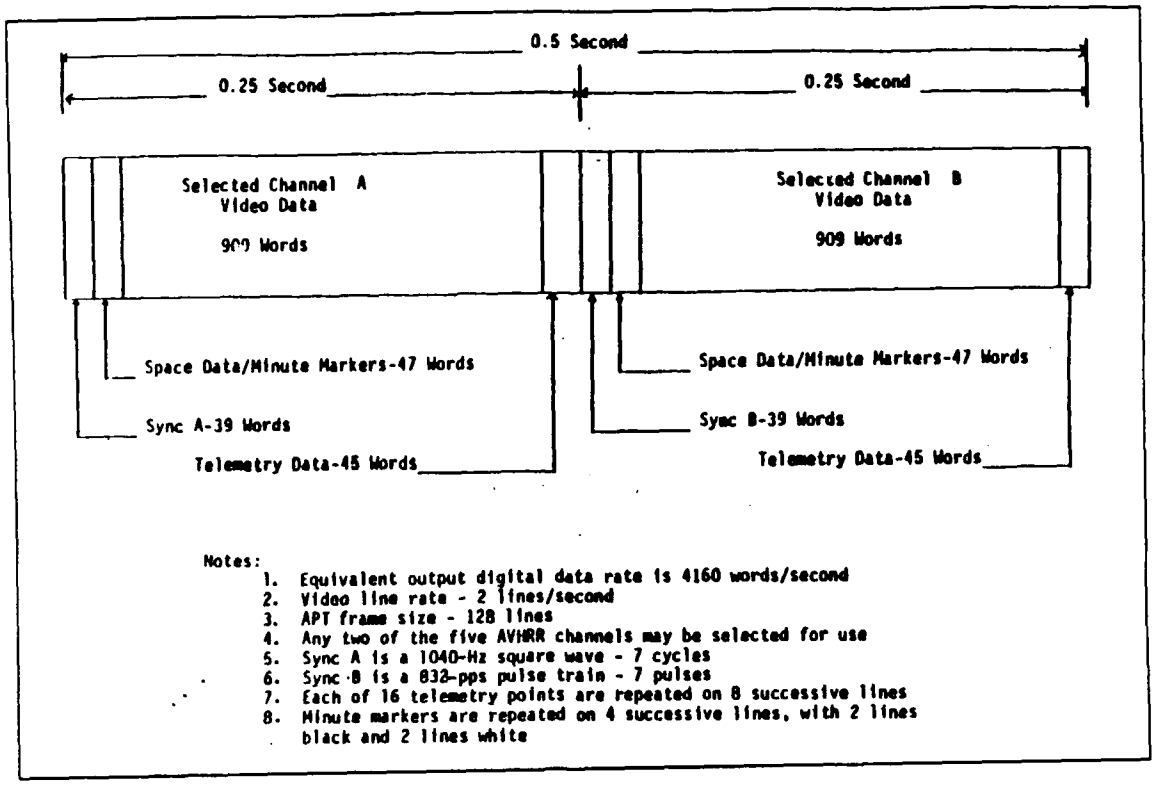

Figure 9. APT Line Format [10:14]

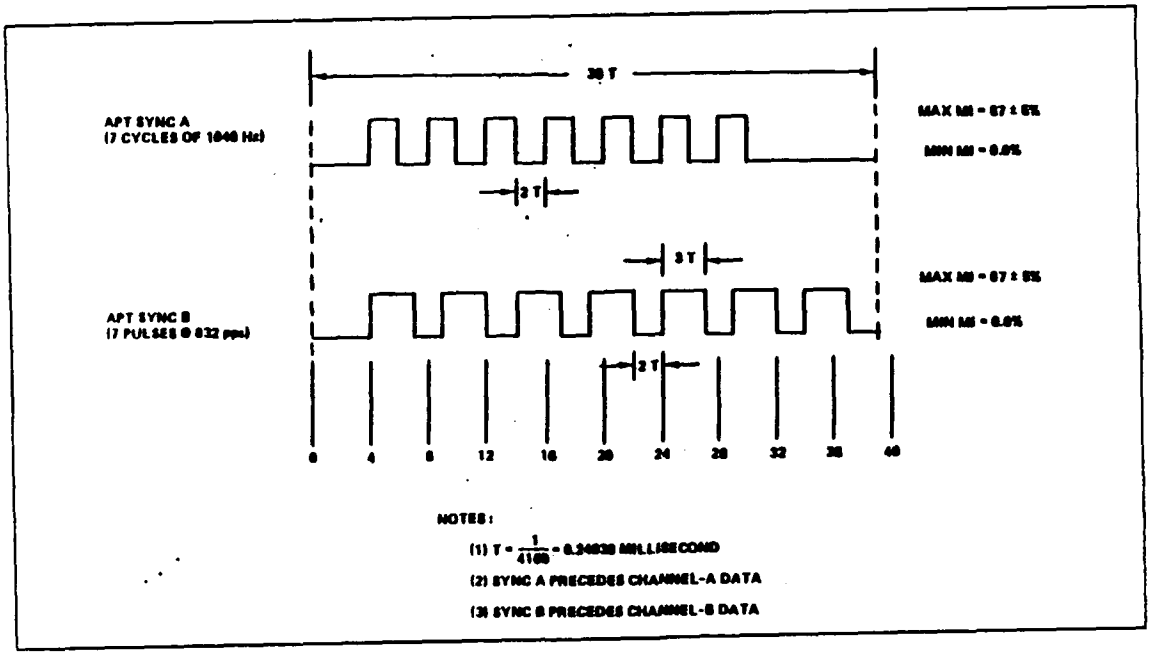

Figure 10. APT Synchronization Format [10:16]

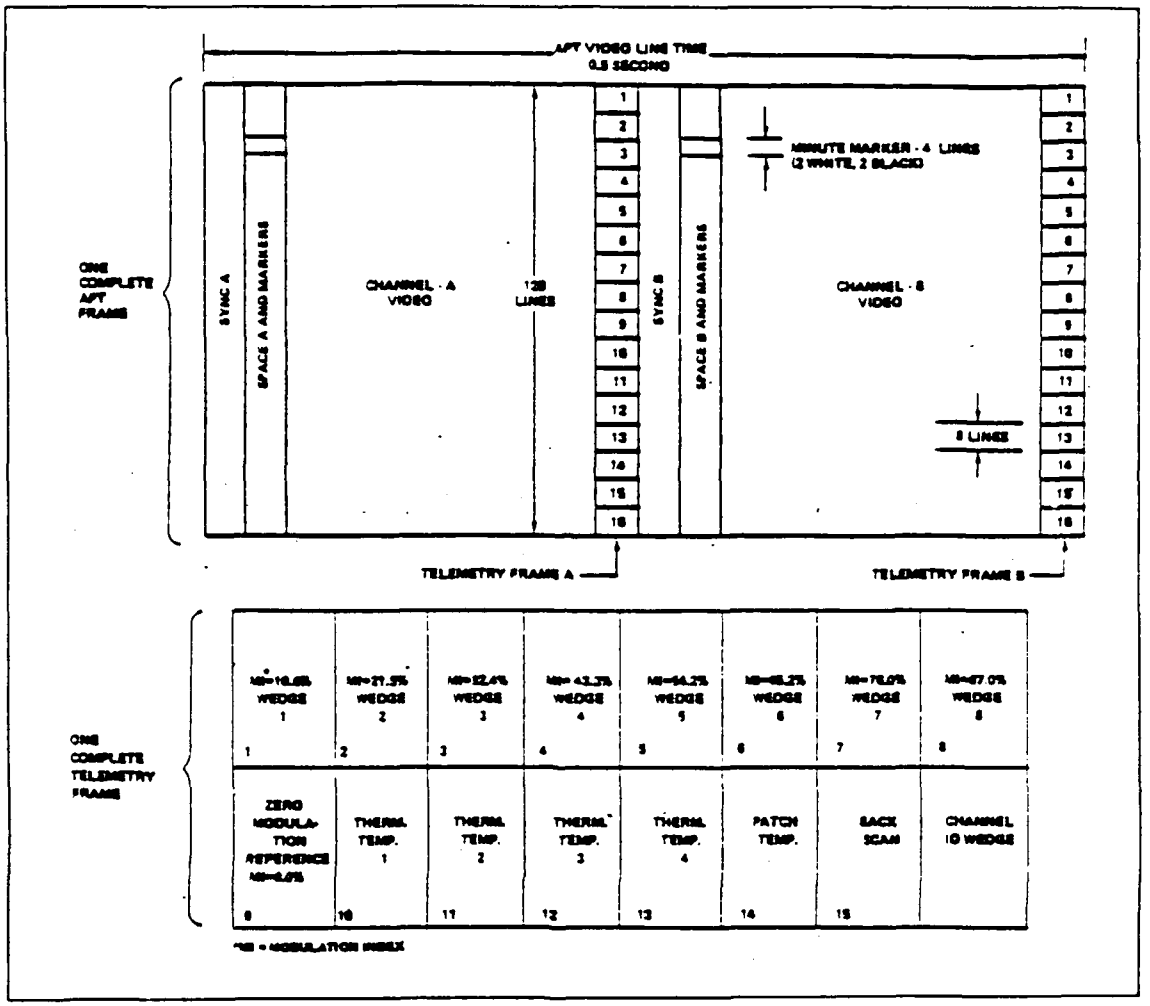

Figure 11. APT Frame Format [10:15]

the analog signal at regular intervals and assigning a digital value to the amplitude measured. Comparing digital HRPT data and digitized APT data has shown good correlation [21]. It should be noted that the digital information derived is an approximate representation of the original APT digital data before conversion to analog. The best possible case would be synchronized sampling at the APT data rate (4160 Hz) to recover the 8 MSBs of the original 10-bit

words. A sample rate higher (or lower) than the data rate has the effect of interpolating (or smoothing) the data.

For this study, a sampling rate of 9600 Hz was used. The resulting 4800 samples per line represent an interpolation of the original 2080 words per line. At this sampling rate, the ratio of samples to words is 30:13 (2.3077:1).

Earth/Satellite Viewing Geometry

The basic earth/satellite viewing geometry lies in a plane determined by the satellite position S, earth location E, and earth center O (See Figure 12). The off-nadir viewing angle δ, earth center angle (ECA) Ψ, local zenith angle Z, satellite radius r, and range distance d from satellite S to earth location E are related as shown in the following discussion.

Applying the cosine law in triangle SOE gives

$$R_E^2 = d^2 + r^2 - 2dr\cos\delta \qquad (2)$$

where R_E is the earth radius at location E.
Solving for d and using the negative root (which is the closer distance) relates the range, d, to off-nadir angle δ:

$$d = r\cos\delta - (R_E^2 - r^2 \sin^2\delta)^{1/2} \qquad (3)$$

where r is the satellite radius (from O) and R_E is the earth radius at location E.

The Zenith angle, Z, is an exterior angle of triangle SOE, so that

$$Z = \delta + \Psi \qquad (4)$$

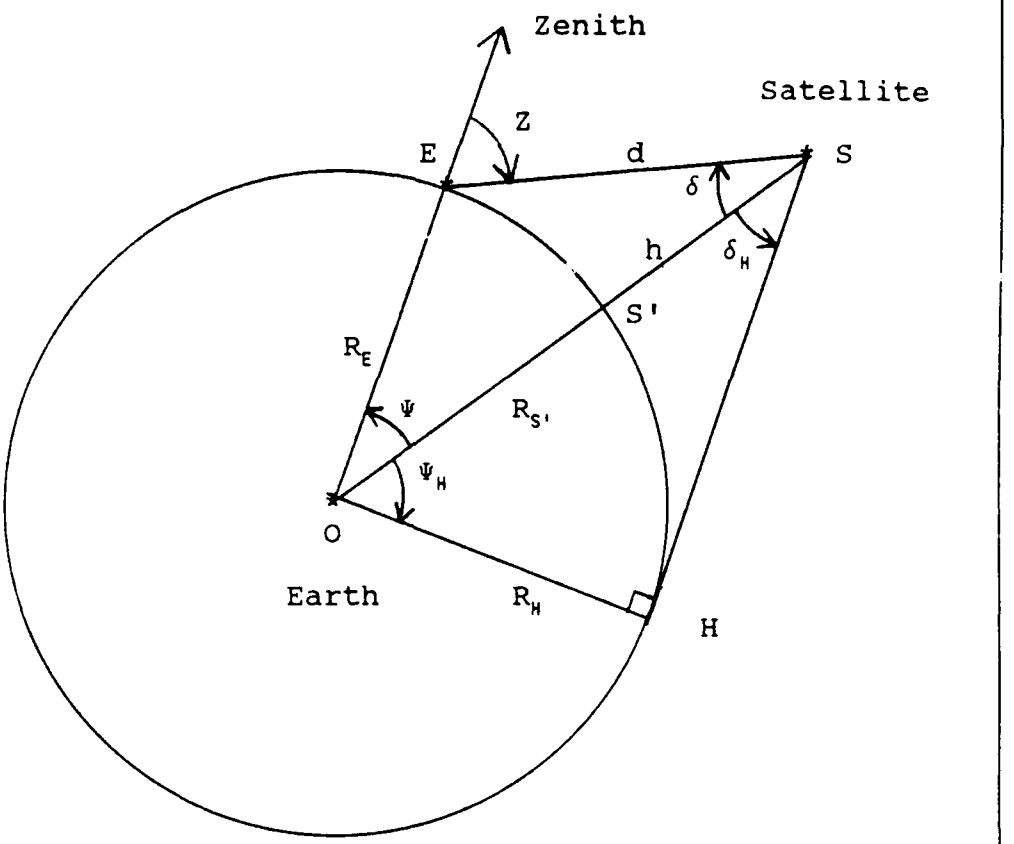

Legend:

Points		Distances	
S:	Satellite	h:	Satellite height
S':	Subpoint	d:	Range from S to E
E:	Earth Location	R:	Earth radius
O:	Earth Center	r:	Satellite radius (r = R + h)
H:	Earth Horizon		

Angles

δ:	Off-nadir angle
Ψ:	Earth Center Angle (ECA)
Z:	Zenith angle

Figure 12. Earth/Satellite Viewing Geometry

Applying the law of sines in plane triangle SOE also yields

$$\sin Z = (r/R_E)\sin\delta \tag{5}$$

Substituting Equation 4 into Equation 5 gives

$$\sin(\delta + \Psi) = (r/R_E)\sin\delta \tag{6}$$

Using the identity $\sin(A+B) = \sin A\cos B + \cos A\sin B$ in Equation 6 gives δ in terms of Ψ:

$$\tan\delta = \sin\Psi/[(r/R_E) - \cos\Psi)] \tag{7}$$

Combining Equations 3 and 6 relates d to δ and Φ:

$$d = r\cos\delta - R_E\cos(\delta + \Psi) \tag{8}$$

These general relations are valid regardless of the shape of the earth or the path of the satellite. The following sections will apply these relations.

Reception, Coverage, and Resolution

The relations above make no assumptions about the earth's shape or the satellite orbit. To simplify the discussion of satellite reception, coverage, and resolution, in this section the earth is assumed to be a sphere with radius R = 6371 km and the satellite orbits are circular.

These assumptions are accurate to a first approximation. The earth radius only varies from about 6378 km at the equator to 6357 km at the poles [10:C-10]. This difference is within $\pm$15 km (0.235%) of the mean. The TIROS-N satellite heights vary by less than 56 km (6.5%) [15:21].

The satellite track and footprint are illustrated in Figure 13. The subpoint latitude and longitude are related

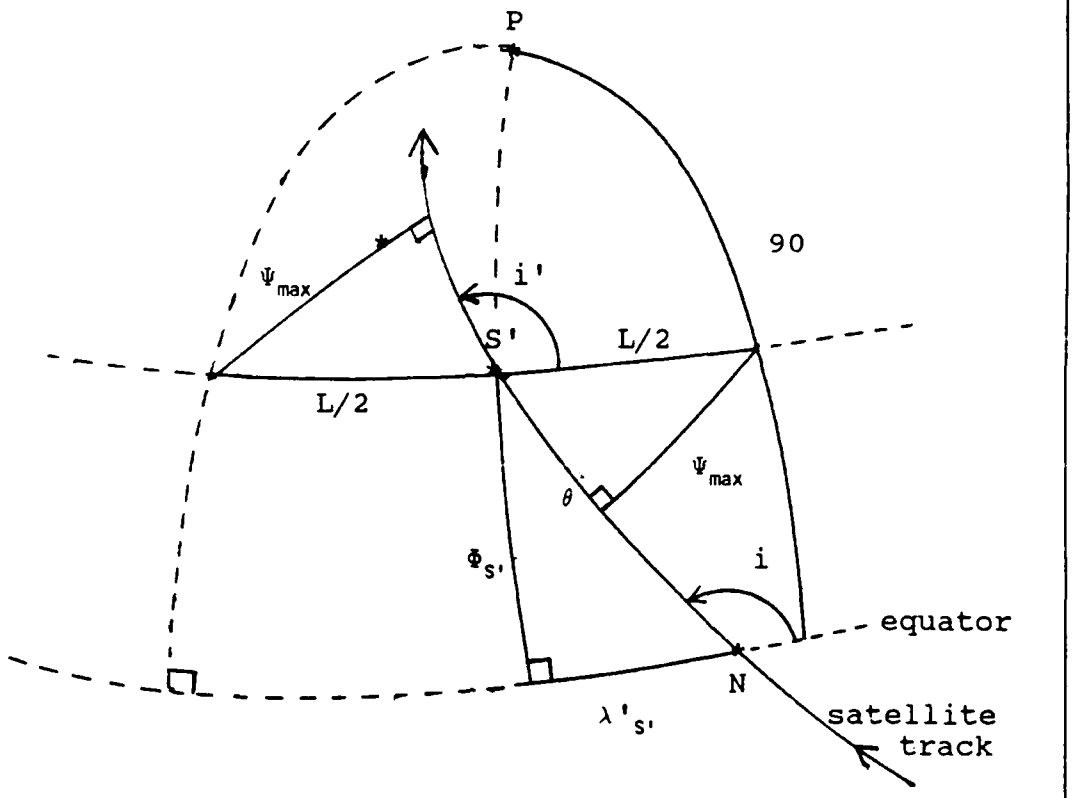

Legend

Points		Angles	
E:	Earth location	i:	Orbital inclination
S':	Satellite subpoint	i':	Latitude crossing angle at subpoint S'
N:	Ascending node at static longitude		
P:	North pole (rotational)		

Arcs

- Φ: latitude
- λ': static longitude from N
- Ψ: Earth Center Angle (ECA)
- θ: Great circle arc from N to S'
- L: Footprint departure (small circle arc)

Figure 13. Satellite Track and Footprint

to the angular distance traveled by the satellite after equator crossing as follows:

$$\sin\Phi_{s'} = \sin\theta \sin(i) \tag{9}$$

$$\sin\lambda'_{s'} = \cos\theta/\cos\Phi \tag{10}$$

where

$\Phi_{s'}$ = subpoint latitude
$\lambda'_{s'}$ = static subpoint longitude measured from the ascending node
θ = angular distance from the ascending node to the satellite subpoint
i = orbit inclination

The static longitude is measured from the fixed position of the ascending node. This provides a convenient reference for geometric purposes. Since the earth rotates, the static longitude of any point on the surface changes with time.

The satellite crosses the parallel of latitude $\Phi_{s'}$ at an angle i':

$$\cos(i') = \sin\lambda'/\sin\theta \tag{11}$$

The departure is the small circle distance between two points along a given parallel of latitude. The departure L at latitude Φ can be approximated with a great circle arc by

$$\sin(L/2) = \sin\Psi_{max}/\sin(i') \tag{12}$$

where

Ψ_{max} = maximum earth center angle
i' = latitude crossing angle

This is used below to calculate satellite coverage.

Reception. Since APT reception is essentially line-of-sight, the satellite is only visible to a ground station when above the local horizon [17:7-6]. In other words, reception begins when the zenith angle decreases to 90 degrees and the satellite rises. This situation is illustrated as triangle SOH in Figure 12.

Denoting horizon values by the subscript H, the earth center angle, Ψ_H, is given by $\cos\Psi_H = R_H/r$. Assuming a spherical earth with mean radius of 6371 km and nominal satellite heights of 833 km and 870 km, this gives ECA Ψ_H values of 27.80 deg (0.4857 rad) and 28.38 deg (0.4952 rad), respectively. Using Equation 3, these correspond to off-nadir δ_H values of 62.18 deg and 61.62 deg.

The great circle distance from earth location H to subpoint S' is $R\Psi_H$, where Ψ_H is in radians. Using the Ψ_H values previously calculated gives horizon distances of 3,094 km and 3,155 km for the nominal satellite heights of 833 km and 870 km, respectively.

So, the satellite is visible whenever the suborbital track lies within a radius of about 3,094-3,155 km from the earth station. In general, the higher the satellite, the greater the visibility.

Coverage. The coverage of a given earth location (the frequency with which it is visible to the satellite sensors) depends on the swath width of each earth scan and the dis-

tance the track shifts on each orbit. Swath width is determined by the satellite height and maximum scan angle, while track displacement is determined by the orbital inclination and period.

As noted previously, the maximum AVHRR scan angle is ± 55.4 deg from nadir. Using Equation 4 with the nominal satellite altitudes of 833 km and 870 km gives Ψ values of ± 13.15 deg and ± 13.92 deg, respectively. These correspond to earth surface distances of ± 1,463 km and ± 1,547 km from the satellite subpoint (swath widths of 2,926 km and 3,094 km).

Recall that the satellite is visible at an earth station at distances up to 3,094-3,155 km from subpoint. This means that the satellite may be visible to an earth station without providing sensor coverage of that location.

Since data can be received when the satellite is within a circle surrounging the station, maximum coverage is available to stations on the satellite track, as illustrated in Figure 14. This provides coverage of an area about 3,000 km x 6,250 km (18,750,000 km^2) centered at the earth station.

The longitude distance spanned by each swath at the equator is slightly greater than the swath width due to the orbit inclination (see Figure 13). Using a nominal inclination of 98.8 deg and swath widths of 2,926 km and 3,094 km, solving Equation 13 gives longitude widths at the equator

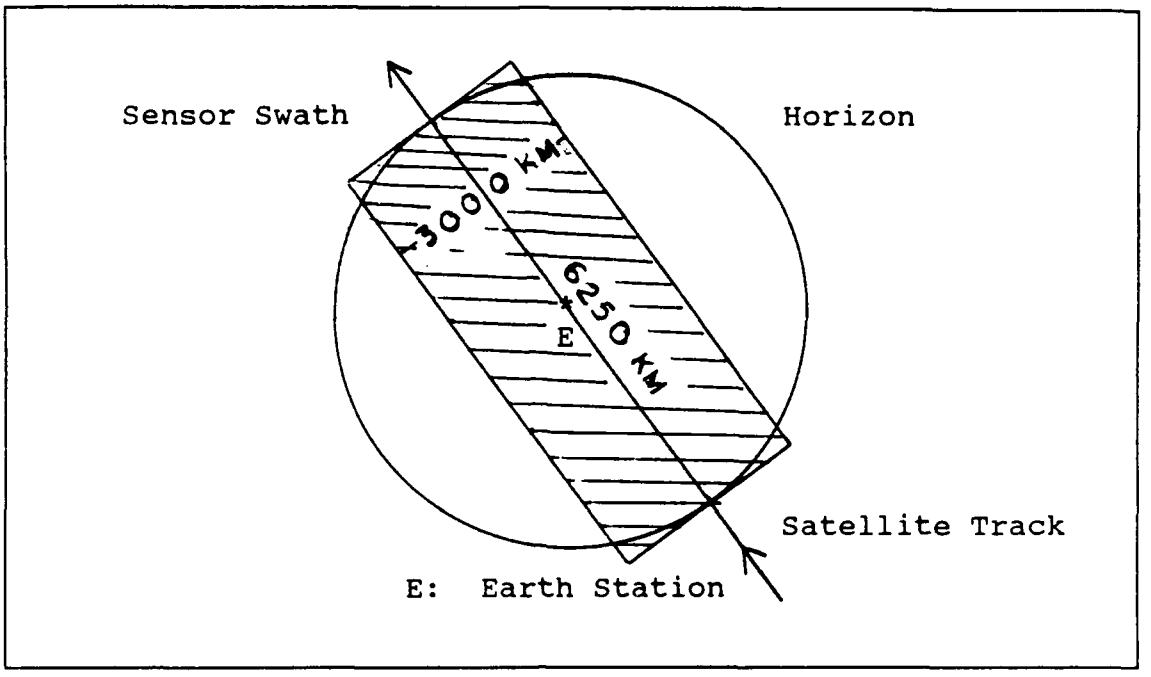

Figure 14. Maximum AVHRR Sensor Coverage

of 26.31 deg and 28.09 deg, or 2,960 km and 3,134 km, respectively.

As discussed earlier (see Earth Characteristics), the eastern rotation of the earth causes the satellite track to shift westward at the rate of 15.0411 deg/hr. For a nominal satellite period of 102.37 min, this amounts to an increment of 25.59 degrees of longitude per orbit. With a swath spanning about 28.09 deg longitude at the equator, each earth location is covered at least twice each day (one ascending pass and one descending pass).

The departure (distance between degrees of longitude along constant latitude) varies with latitude Φ in propor-

tion to cosΦ [12:39]. Thus, the higher the latitude, the less the westward shift due to rotation.

The longitude difference $\Delta\lambda$ spanned by a given departure L is

$$\Delta\lambda = L/\cos\Phi \tag{13}$$

On average, the number of passes per day that cover an earth location at latitude Φ is

$$(\text{passes/day}) = (\text{orbits/day})\Delta\lambda/180 \tag{14}$$

Solving Equations 12, 13, and 14 gives the satellite coverage (passes/day) for both satellite reception and sensor coverage using the appropriate maximum ECA values (Ψ_{max}).

The average number of reception and coverage passes per day are given in Table 14 at various latitudes for a nominal 870 km orbit. These are approximate values only. The results of a computer simulation over a 30 day period produced similar data, though deviations up to 1 pass/day were noted at higher latitudes.

Resolution. The resolution of a pixel is the size of an area on the earth's surface that just fills the IFOV of the sensor. This depends on the angular IFOV, range from satellite to the area imaged, and image skew due to off-nadir viewing and the curvature of the earth.

The IFOV can be expressed as the difference in scan angle between the beginning and the end of a pixel.

Table 14. Earth Station Daily Coverage by Latitude

Latitude degrees (N/S)	Coverage passes/day	Reception passes/day
0	2.2	4.5
15	2.3	4.7
30	2.5	5.2
40	2.9	5.9
50	3.5	7.1
60	4.6	9.4
70	7.1	14.1
75	10.5	14.1
80	14.1	14.1
$\geq$ 81.1	14.1	14.1

Denoting pixel beginning and end by subscripts 1 and 2, respectively, the IFOV is then $\Delta\delta = \delta_2 - \delta_1$.

Solution of Equation 6 for Ψ_1 and Ψ_2 yields an ECA value of $\Delta\Psi = \Psi_2 - \Psi_1$. Referring to Figure 2, the along-line resolution, ΔL, is approximately $R\Delta\Psi/\cos\gamma$ where γ is the scan skew.

Thus, the AVHRR IFOV of 1.3 mr corresponds to HRPT nadir resolutions of 1.08 km and 1.13 km for the nominal satellite heights of 833 km and 870 km, respectively. Along-line resolution decreases progressively with increasing scan angle as illustrated in Figure 15 for a nominal

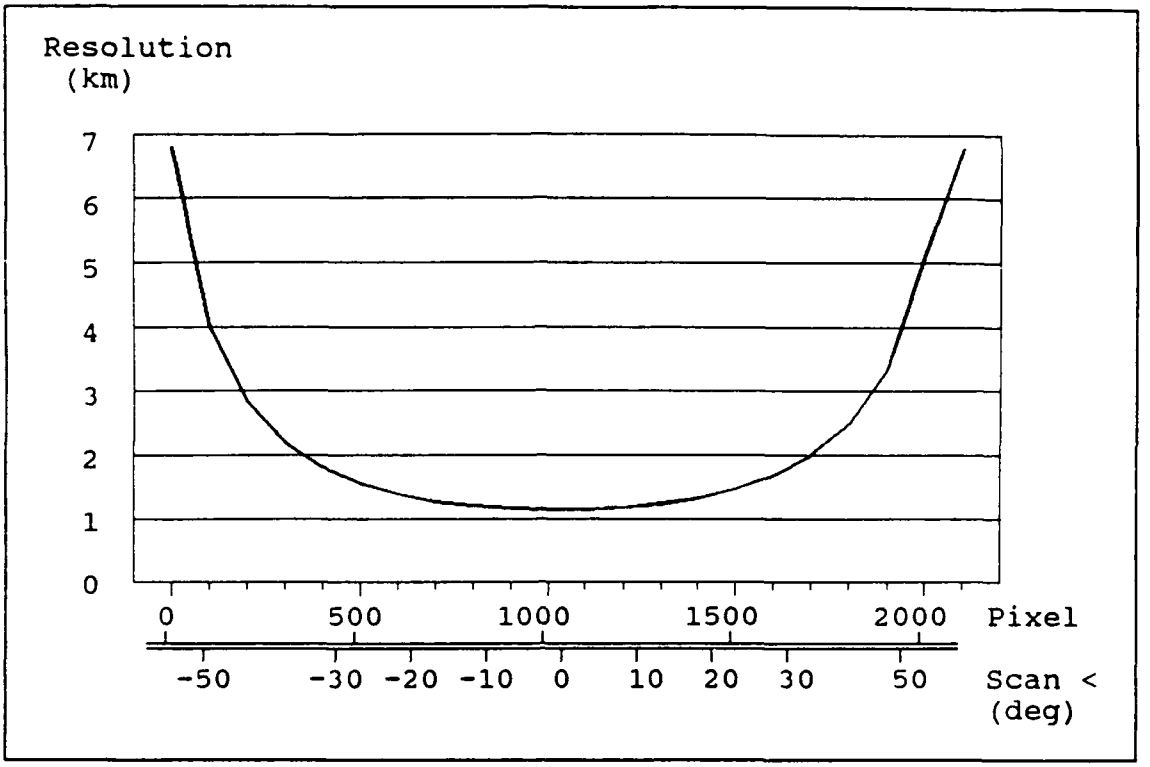

Figure 15. HRPT Along-Line Resolution

satellite height of 870 km with earth radius of 6378.14 km.

APT processing reduces resolution along the scan line by averaging HRPT pixels. Because of IFOV overlap with consecutive pixels (see Figure 6), the IFOV of an APT pixel averaged from n HRPT pixels is

$$IFOV_{APT} = (n - 1)STEP + IFOV_{HRPT} \quad (15)$$

where STEP is the mirror step size for each AVHRR word. Recall that each step is 25 timing counts, so that STEP = 0.94439882 mr.

The HRPT/APT reduction algorithm in Table 7 produces a nearly uniform resolution of 4 km along the scan line as

illustrated in Figure 16. The AVHRR IFOV of 1.3 mr corresponds to APT subpoint resolutions of 3.44 km and 3.59 km for the nominal satellite heights.

Because of the varying size of HRPT pixel images along the scan line, some sort of data resampling is required for HRPT to remove distortion. Repeating pixels in inverse proportion to their resolution is one method, as presented by Emery [3:1177]. Since APT scan lines have nearly uniform resolution, data resampling should not be required for APT.

Subsequent HRPT scan lines are nominally contiguous at the subpoint [15:43]. The line width is given by the forward progress of the satellite during one scan line. For a nominal satellite period of 102 min and AVHRR scan rate of 6 lines/sec, this corresponds to an ECA of 0.00980 deg (0.171 mr). Using Equation 13, the HRPT line width is about 1.09 km.

Similarly, the APT line rate of 2 lines/sec corresponds to an APT line width of about 3.27 km. It should be noted that each APT line is actually the data from one in three AVHRR lines. The other two lines are missing in APT. If the APT lines are represented as contiguous, there is an implicit repetition of one AVHRR/APT line three times.

Denoting line width as along-track resolution, the APT and HRPT subpoint resolutions are summarized in Table 15.

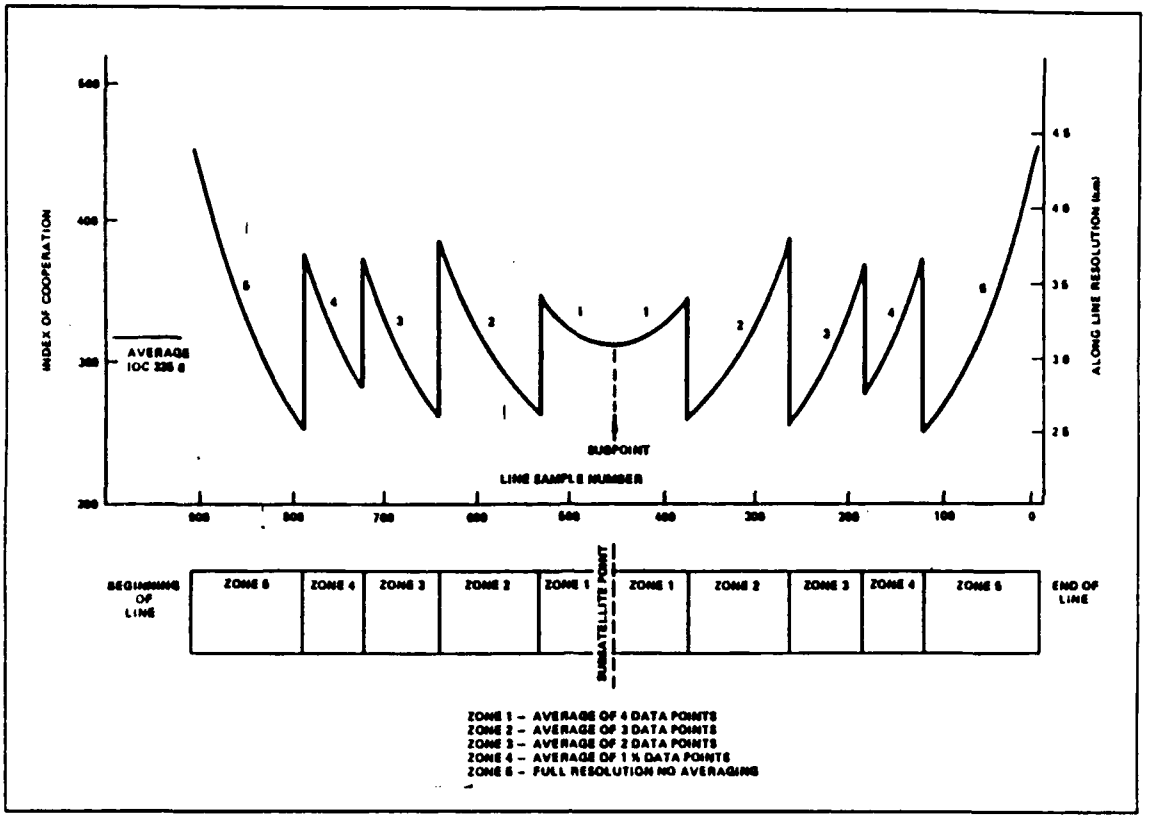

Figure 16. APT Along-Line Resolution [15:17]

Table 15. HRPT/APT Subpoint Resolution

	Along-Line (km)	Along-Track (km)
HRPT	1.08-1.13	1.09
APT	3.44-3.59	3.27

The along-track resolution is also reduced with increasing scan angle due to the increasing range from satellite to image area and the earth's curvature.

Earth Location of Pixel Images

The earth scene viewed in each pixel represents a square view of a spheroid earth, generally from a skewed viewing angle. In general, the area viewed will have an irregular shape that is different for each pixel.

Here, the location of a pixel will be defined as the earth location in the center of the pixel IFOV. Assuming that the earth scene is essentially flat in the pixel IFOV, this location also corresponds to the center of the earth area viewed. Each pixel is then associated with a unique earth location. The following chapter shows how to determine the earth location of each pixel and to find the pixel that contains a view of a given earth location.

IV. Spatial Registration

Introduction

Spatial registration relies on the fact that each pixel is directly related to an earth location by the satellite position, earth position, and sensor scan angle. Knowing these relations as functions of time allows transformation from pixel coordinates to geographic coordinates (direct referencing) and vice versa (inverse referencing).

The most critical factor in spatial registration is timing. At an AVHRR sensor scan rate of six lines per second, a timing error of one second in the computed satellite position is equivalent to an error of six AVHRR lines (6.54 km at the satellite subpoint). To account for this, provision should be made for a time adjustment in the reference time, t_0 (see Equation 46).

To make this time adjustment prior to direct registration, the inverse registration algorithm can be used to overlay a geographic outline on the satellite image. The reference time can then be adjusted to improve the registration visually. Once a more accurate reference time is obtained, the entire image can be accurately registered using the direct referencing algorithm.

First, this chapter explores the general relationships. Second, various coordinate transformations necessary to relate different coordinate systems are presented. Finally, specific registration algorithms are introduced for both direct and inverse image referencing.

Notation

In this chapter, the following notation is observed:

$\underline{r}$ = vector

r = scalar magnitude of vector $\underline{r}$

$\hat{\underline{r}}$ = unit vector in direction of $\underline{r}$ ($\hat{\underline{r}} = \underline{r}/r$)

r_x, r_y, r_z = scalar components of $\underline{r}$ ($\underline{r} = \hat{\underline{x}}r_x + \hat{\underline{y}}r_y + \hat{\underline{z}}r_z$)

$\underline{r} \times \underline{v}$ = vector cross product of $\underline{r}$ and $\underline{v}$

$\underline{r} \cdot \underline{v}$ = scalar dot product of $\underline{r}$ and $\underline{v}$

All vectors are referenced to an inertial coordinate system (Earth Centered Inertial) with origin, O, at the center of the earth, and unit vectors defined as follows:

$\hat{\underline{x}}$ = direction from O toward the first point of Aries (star reference)

$\hat{\underline{y}}$ = direction from O in the plane of the earth's equator such that $\hat{\underline{x}} \times \hat{\underline{y}} = \hat{\underline{z}}$ (right-hand coordinate system)

$\hat{\underline{z}}$ = direction from O toward the earth's north pole

General Relationships

In the Earth Centered Inertial (ECI) coordinate system described above, the pixel earth location is determined by the satellite velocity and range vectors by the following (see Figure 17):

$$\underline{R} = \underline{r} + \underline{d} \tag{16}$$

where

$\underline{R}$ = earth location vector
$\underline{r}$ = satellite position vector
$\underline{d}$ = range vector from satellite to earth location

All three vary in time. If the satellite position $\underline{r}$ is known as a function of time, then given either $\underline{R}$ or $\underline{d}$ at a given time, the other can be computed with Equation 16.

Define the scan vector $\underline{s}$ in Figure 17 by

$$\underline{s} = \underline{r} \times \underline{v} \tag{17}$$

where $\underline{v}$ is the satellite velocity vector. Note that the unit vector $\hat{s}$ represents the scan direction (right to left).

The off-nadir scan angle δ determines the range direction $\hat{d}$ from $\hat{r}$ and $\hat{s}$:

$$\hat{d} = -\hat{r}\cos\delta + \hat{s}\sin\delta \tag{18}$$

Recall that Equation 3 gives the range distance d:

$$d = r\cos\delta - (R^2 - r^2\sin^2\delta)^{1/2} \tag{19}$$

Thus, combining Equations 18 and 19 with the vector identity $\underline{d} = \hat{d}d$ yields an expression for $\underline{d}$ in terms of δ:

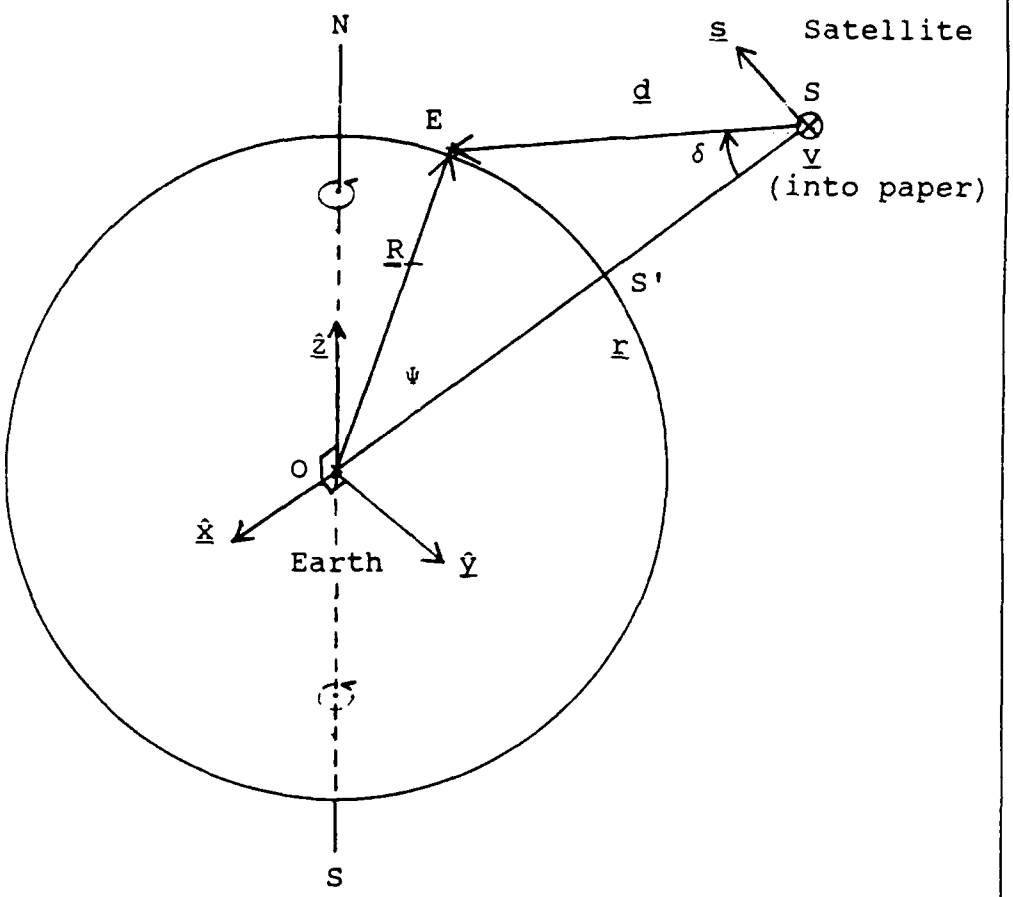

Legend:

Points		Vectors	
S:	Satellite	r:	Satellite position
S':	Subpoint	d:	Range from S to E
E:	Earth location	R:	Earth position
O:	Earth center		

Angles		Directions	
δ:	Off-nadir scan angle	x̂:	to Aries
Ψ:	Earth Center Angle (ECA)	ŷ:	90 deg East of x̂
		ẑ:	north

Figure 17. Satellite/Earth Geometry (ECI Coordinates)

$$d = -\hat{r}\{\cos\delta[r\cos\delta - (R^2 - r^2\sin^2\delta)^{1/2}]\}$$
$$+ \hat{s}\{\sin\delta[r\cos\delta - (R^2 - r^2\sin^2\delta)^{1/2}]\} \quad (20)$$

Spherical Earth. If a spherical earth is assumed, the earth radius R is a known constant. Substituting Equation 20 into Equation 16 then gives the desired earth location $\underline{R}$.

Oblate Spheroid Earth. For an oblate spheroid earth, however, the earth radius R is a function of latitude. An expression for R is therefore required in terms of the satellite radius, velocity, and scan angle.

Each point (R_x, R_y, R_z) on an earth meridian ellipse satisfies the relation

$$(R_x^2 + R_y^2)/R_{eq}^2 + R_z^2/R_{po}^2 = 1 \quad (21)$$

where R_{eq} and R_{po} are the earth equatorial and polar radii, respectively. Substituting the Pythagorean relation $R_x^2 + R_y^2 = R^2 - R_z^2$ into Equation 21 and solving for R^2 gives

$$R^2 = R_{eq}^2 - \xi R_z^2 \quad (22)$$

where

$$\xi = R_{eq}^2/R_{po}^2 - 1 \quad (23)$$

Note that $\xi = e^2/(1 - e^2)$ where e is the eccentricity of the meridian ellipse.

From Equation 16, $R_z = r_z + d_z = r_z + d\hat{d}_z$. Substitution into Equation 22 yields

$$R^2 = R_{eq}^2 - \xi(r_z + d\hat{d}_z)^2 \quad (24)$$

Recall from Equation 1 that

$$R^2 = r^2 + d^2 - 2rd\cos\delta \qquad (25)$$

Combining Equations 24 and 25 then rearranging produces

$$d^2(1 + \xi\hat{d}_z^2) - 2d(r\cos\delta - \xi r_z\hat{d}_z) = R_{eq}^2 - r^2 - \xi r_z^2 \qquad (26)$$

Solving for d by taking the negative root (closer range), gives

$$d = r\cos\delta - \xi r_z\hat{d}_z/(1 + \xi\hat{d}_z^2) - \{[R_{eq}^2 - r^2 - \xi r_z^2 + (r\cos\delta - \xi r_z\hat{d}_z)^2]/(1 + \xi\hat{d}_z^2)\}^{1/2} \qquad (27)$$

The range vector is again derived by applying the relation $\underline{d} = d\underline{\hat{d}}$ to Equations 18 and 27.

Satellite Position

For these registration methods, highly accurate satellite positions are required. This section will briefly discuss the general orbital case and a local approximation to simplify the numerical calculations.

Elliptical Orbits. In general, the satellite will follow an elliptical orbit with one focus at the center of the earth. Perturbations caused by the earth's equatorial bulge, drag, and the gravitational attractions of the sun and moon will alter the orbit over time. To get an accurate satellite position at a time after epoch (time the satellite position was measured), an elliptical orbit model with perturbations should be used. The registrations in this work used satellite position calculations produced by an

elliptical orbit program based on the NORAD SGP (Simplified General Perturbations) model.

Spherical Orbit Approximations. Over small periods of time, the satellite motion may be approximated by a spherical orbit. The following discussion shows how approximate satellite position and velocity vectors may be calculated in the vicinity of an initial set of accurate satellite position and velocity vectors.

For a satellite in a circular orbit at radius r, the satellite circular velocity, v_c, is given by [2:34]

$$v_c = (\mu/r)^{1/2} \tag{28}$$

where

μ = earth gravitational constant ($3.98600448 \times 10^{14}$ $m^3 s^{-2}$ [20:K6]).

A local approximation for the satellite angular velocity, $\dot{\theta}$, is obtained by combining Equation 28 with the relation $v_c = r\dot{\theta}$:

$$\dot{\theta} = (\mu/r^3)^{1/2} \tag{29}$$

For a spherical orbit, the angular speed is simply

$$\dot{\theta} = 2\pi/P \tag{30}$$

where P is the orbit period.

The circular velocity vector, $\underline{v}_c$, is given by

$$\underline{v}_c = (-\hat{\underline{r}} \times \hat{\underline{h}})v_c \tag{31}$$

where

$\underline{r}$ = satellite radius vector
$\underline{v}$ = satellite velocity vector

$\underline{h}$ = angular momentum vector ($\underline{r}$ x $\underline{v}$)
v_c = circular velocity from Equation 28

Given the satellite position $\underline{r}(t)$ and velocity $\underline{v}(t)$ at time t, the satellite position vector $\underline{r}(t + \Delta t)$ and velocity vector $\underline{v}(t + \Delta t)$ at time $t + \Delta t$ can be approximated using a circluar orbit. It can be shown that they are given by [2:72]

$$\underline{r}(t + \Delta t) = \underline{r}(t)[\cos(\dot{\theta}\Delta t)] + \underline{v}_c(t)[\sin(\dot{\theta}\Delta t)/\dot{\theta}] \quad (32)$$

and

$$\underline{v}_c(t + \delta t) = -\hat{\underline{r}}(t)\{[v_c(t)/r]\sin(\dot{\theta}\Delta t)\} + \underline{v}_c(t)[\cos(\dot{\theta}\Delta t)] \quad (33)$$

where

$\underline{v}_c(t)$ = circular velocity vector given by Equation 31
$\dot{\theta}$ = satellite angular velocity given by Equation 29

The above equations can be used in the direct referencing algorithm to calculate satellite and subpoint positions more quickly, instead of using elliptical model calculations for every pixel.

Pixel Time

The general relations above show how the earth location vector is determined by the satellite position and velocity vectors and the sensor scan angle at a given time. This is sufficient for direct referencing since the pixel time is known.

For inverse referencing, the earth location is known, but not the time of the pixel which views that location. This time is found using an iterative procedure by estimating the time that the scan vector will cross the earth location in question, assuming no earth rotation. Updating the earth position (in static coordinates) by accounting for earth rotation, and repeating the process produces increasingly better time estimates.

For the purpose of simplification, assume that the earth is spherical and the satellite orbit circular. Referring to Figure 18, let the earth location and satellite subpoint geocentric coordinates (λ,Φ) be denoted by the subscripts E and S', respectively.

The first step is to find the equivalent time and longitude of the ascending node N (equator crossing), assuming a spherical orbit. If the orbit is truly circular, these will be the actual values.

Given the geocentric latitude $\Phi_{S'}$ and longitude $\lambda_{S'}$ for subpoint S' at time $t_{S'}$ (the center of the image is good), Equation 9 can be rewritten to give the satellite orbit angle, $\theta_{S'}$, from equator crossing:

$$\sin\theta_{S'} = \sin\Phi_{S'}/\sin(i) \qquad (34)$$

where $\dot{\theta}$ = orbit angular velocity, given by Equation 30 (spherical orbit) or Equation 29 (spherical approximation).

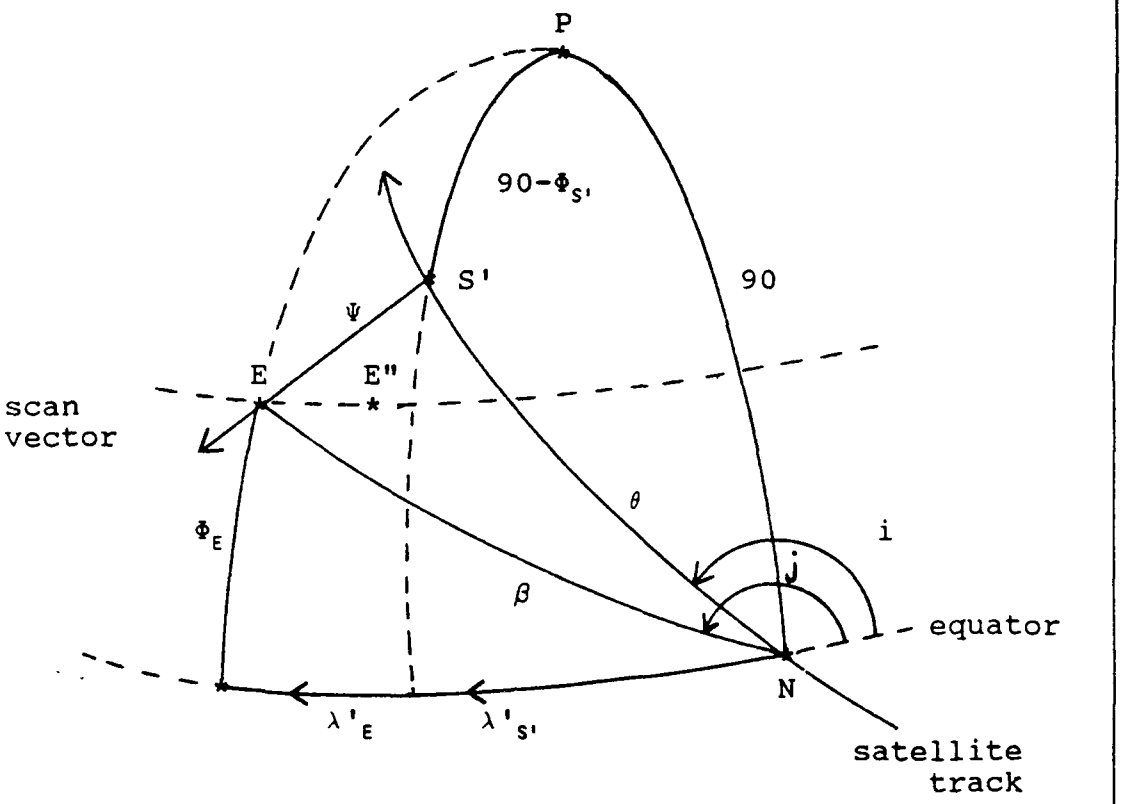

Legend

Points		Angles	
E:	Earth location	i:	Orbital inclination
E':	Projected E location	j:	Angle from the equator to E (great circle)
S':	Satellite subpoint		
N:	Ascending node at static longitude		
P:	North pole (rotational)		

Arcs

Φ:	latitude
λ':	static longitude
Ψ:	Earth Center Angle (ECA)
θ:	Great circle arc from N to S'
β:	Great circle arc from N to E

Figure 18. Satellite Track/Scan Geometry (Static)

The time of the ascending node, t_N, is then

$$t_N = t_{S'} - \theta_{S'}/\dot{\theta} \tag{35}$$

The subpoint static longitude, $\lambda'_{S'}$, is given by

$$\cos(\lambda'_{S'}) = \cos\theta_{S'}/\cos\Phi_{S'} \tag{36}$$

The longitude, λ_N, of the ascending node N can now be computed as follows:

$$\lambda_N = \lambda_{S'} + \lambda'_{S'} - (t_{S'} - t_N)(\Omega - \dot{\Lambda}) \tag{37}$$

where

Ω = earth rotation rate (0.2506845 deg/min)
$\dot{\Lambda}$ = orbital precession rate (6.844774×10^{-4} deg/min for sun-synchronous orbits)

Given an earth location E at geocentric coordinates (Φ_E, λ_E), the next step is to guess a viewing time t_E (use the subpoint time, $t_{S'}$, or any central time). The static longitude of E, λ'_E, is then given by

$$\lambda'_E = \lambda_N - \lambda_E + (t_E - t_N)(\Omega - \dot{\Lambda}) \tag{38}$$

Values for β, j, and Ψ are then computed using trigonometric relations in Figure 18:

$$\cos\beta = \cos\Phi_E \cos\lambda'_E \tag{39}$$

$$\sin(j) = \sin\Phi_E / \sin\beta \tag{40}$$

$$\sin\Psi = \sin(j-i)\sin\beta \tag{41}$$

where

β = great circle arc from ascending node N to earth location E

j = angle between the equator and the great circle through N and E

Ψ = earth center angle between subpoint S' and earth location E

Let S" be the projected subpoint location where the scan vector $\underline{s}$ crosses earth location E. The satellite orbit angle, $\theta_{S"}$, at subpoint S" is given by applying the cosine law in triangle ENS":

$$\cos\theta_{S"} = \cos\beta/\cos\Psi \tag{42}$$

The projected scan time, $t_{S"}$, is then

$$t_{S"} = t_N + \theta_{S"}/\dot{\theta} \tag{43}$$

During the time between $t_{S"}$ and t_E, however, the earth location actually moves (in static coordinates) to position E" (see Figure 18). The projected time $t_{S"}$ can then be improved by estimating a new scan crossing time, t', and repeating the calculations above. The new estimate t' is chosen as

$$t' = t_E + \alpha(t_{S"} - t_E) \tag{44}$$

where α is a convergence constant chosen to optimize convergence efficiency.

For an inclination over 90 degrees, assuming no earth rotation tends to overestimate the crossing time. A good value for α is given by the empirical formula

$$\alpha = 1 + \cos(i)\cos\Phi_E\,(\Omega - \dot{\Lambda})/\dot{\theta} \tag{45}$$

In practice, using a value of $\alpha = 1$ performed nearly as well.

This process is repeated until the time difference is less than some arbitrary value, ϵ; i.e. $|t_{S"} - t_E| < \epsilon$.

This results in an HRPT line accuracy of ϵ/T_l lines, where T_l is the HRPT line period (1/6 sec).

The process above produces the best time estimate under the assumption of a circular orbit in the vicinity of subpoint S'. If greater accuracy is desired, the actual position of subpoint S" at time $t_{S"}$ should be computed using an elliptical orbit model. The iterative process of estimating the scan time is then repeated.

A slight error remains due to the oblate (flattened) shape of the earth. If necessary, this could be corrected by computing the pixel geocentric coordinates at the estimated time using the direct referencing algorithm for an oblate spheroid earth. The time estimate could then be further improved through iteration, comparing the computed earth location to the desired one.

Coordinate Transformations

The general relations above reference Earth Centered Inertial (ECI) coordinates. For spatial registration, pixel and geographic coordinates are desired. The following sections show how to transform between these coordinate systems and ECI coordinates.

Pixel Coordinates. The HRPT data consists of a series of pixels referenced by integer line and pixel numbers (l,p). Pixel numbers range from 0 to 2047, and line numbers from 0 to around 5400.

Line and pixel coordinates (l,p) can be considered as continuous to simplify the mathematical transformation to and from continuous geographic coordinates. The corner of the first pixel in the first line has pixel coordinates (-0.5,-0.5) with its center at (0,0). Pixel (l,p) covers line values (l - 0.5 to l + 0.5) and pixel values (p - 0.5 to p + 0.5).

Define the scan angle δ as negative at the beginning of a scan line, zero at nadir, and positive thereafter. The scan angle δ_p at the center of pixel (l,p) is

$$\delta_p = \text{STEP}(p - 1023.5) \tag{46}$$

where STEP is the mirror step angle for each pixel (0.9439882×10^{-3} rad).

The time $t_{l,p}$ corresponding to pixel (l,p) is given by

$$t_{l,p} = t_0 + T_l (l - l_0) + T_p (p - p_0) \tag{47}$$

where

t_0 = reference time of pixel (l_0, p_0)
T_l = time duration of each line (51.27778×10^{-3} sec)
T_p = time duration of each pixel (0.0250401×10^{-3} sec)

Conversely, given scan angle δ and time t for a particular image point, the line and pixel coordinates are given by

$$p = 1023.5 + \delta/\text{STEP} \tag{48}$$

$$l = l_0 + [t - t_0 - T_p (p - p_0)]/T_l \tag{49}$$

Coordinates l and p will be integers only if the image point happens coincide with the center of pixel (l,p) at time t.

In general, it will not. To find the pixel containing the image point, l and p are rounded to the closest integer. This assumes negligible earth rotation (7.292116×10^{-5} rad/sec) during one scan line (1.215353×10^{-5} rad/line or 0.075 km/line at the equator).

Valid pixel coordinates are -0.5 to 2047.5 for p, and -0.5 to l_{max} + 0.5 for l. Coordinates outside this range represent earth locations not viewed in the data.

To register APT data, a transformation between APT and HRPT pixel coordinates is used as summarized in Table 16. Note that the center of APT pixel (l,p) also has coordinates (l,p) and covers the range (l $\pm$ 0.5, p $\pm$ 0.5).

To used sampled APT data, the pixel number must be converted to its data sample number. The APT data rate is 4160 words/sec. If the data is digitized at 9600 samples/sec, the pixel number should be multiplied by 2.30877 (9600 samples/4160 words).

Inertial/Geocentric Coordinates. It is convenient to reference earth locations by latitude and longitude coordinates. Denote geocentric latitude and longitude by Φ_{gc} and λ_{gc}, respectively. These can be expressed in terms of the components of the ECI earth position vector $\underline{R}$ [10:C-13]:

$$\tan\Phi_{gc} = [R_Z / (R_X^2 + R_Y^2)^{1/2}] \quad (50)$$

$$\tan[\lambda_{gc} + GHA(t)] = \tan(R_Y / R_X) \quad (51)$$

Table 16. APT/HRPT Pixel Coordinate Transformation

Region	HRPT pixels	APT pixels	Transformation *
5	0 to 120	0 to 120	$p_H = p_A (1)$
4	121 to 213	121 to 182	$p_H = p_A (1.5) - 60.5$
3	214 to 379	183 to 265	$p_H = p_A (2) - 162$
2	380 to 709	266 to 375	$p_H = p_A (3) - 418$
1	710 to 1337	376 to 532	$p_H = p_A (4) - 794$
2	1338 to 1667	533 to 642	$p_H = p_A (3) - 261$
3	1668 to 1833	643 to 725	$p_H = p_A (2) + 382$
4	1834 to 1926	726 to 787	$p_H = p_A (1.5) + 745$
5	1927 to 2047	788 to 908	$p_H = p_A (1) + 1139$

Channel A: $l_H = l_A (3) - 1$

Channel B: $l_H = l_A (3)$

* p_H = HRPT pixel; p_A = APT pixel
l_H = HRPT line; l_A = APT line

Note: Because of the overlapping of APT pixels in region 4, the pixel centers are offset from the IFOV center by 0.25 STEP in region 4.

where GHA(t) the Greenwich hour angle at time t. This is computed in reference to the beginning of the year by [10:C-12; 2:99-100]

$$GHA(t) = G_0 + G_1 t_d + \Omega t_h \qquad (52)$$

where

G_0 = GHA at the beginning of the year of time t (deg)
G_1 = daily increase in GHA (0.985647366 deg/day)
t_d = day of the year of time t
Ω = rate of earth rotation (360.9856476 deg/day)
t_h = fractional part of a day in time t

Note that GHA is measured from the Greenwich meridian westward to the first point of Aries. Values of G_0 can be found in the Astronomical Almanac [20] for the current year or calculated in reference to epoch.

Geocentric/Geodetic Coordinates. Map coordinates are usually geodetic (also called geographic). As illustrated in Figure 19, geodetic latitude is based on the local horizon of an oblate earth, while geocentric latitude is based on the center of the earth. Geodetic longitude is the same as geocentric longitude.

Denoting geodetic latitude and longitude by Φ_{gd} and λ_{gd}, respectively, geodetic coordinates are related to geocentric coordinates by [3:1177; 10:C-10]

$$\tan\Phi_{gd} = (R_{eq}/R_{po})^2 \tan\Phi_{gc} \tag{53}$$

$$\lambda_{gd} = \lambda_{gc} \tag{54}$$

where

R_{eq} = Equatorial radius of the earth (6378.144 km)
R_{po} = Polar radius of the earth (6356.759 km)

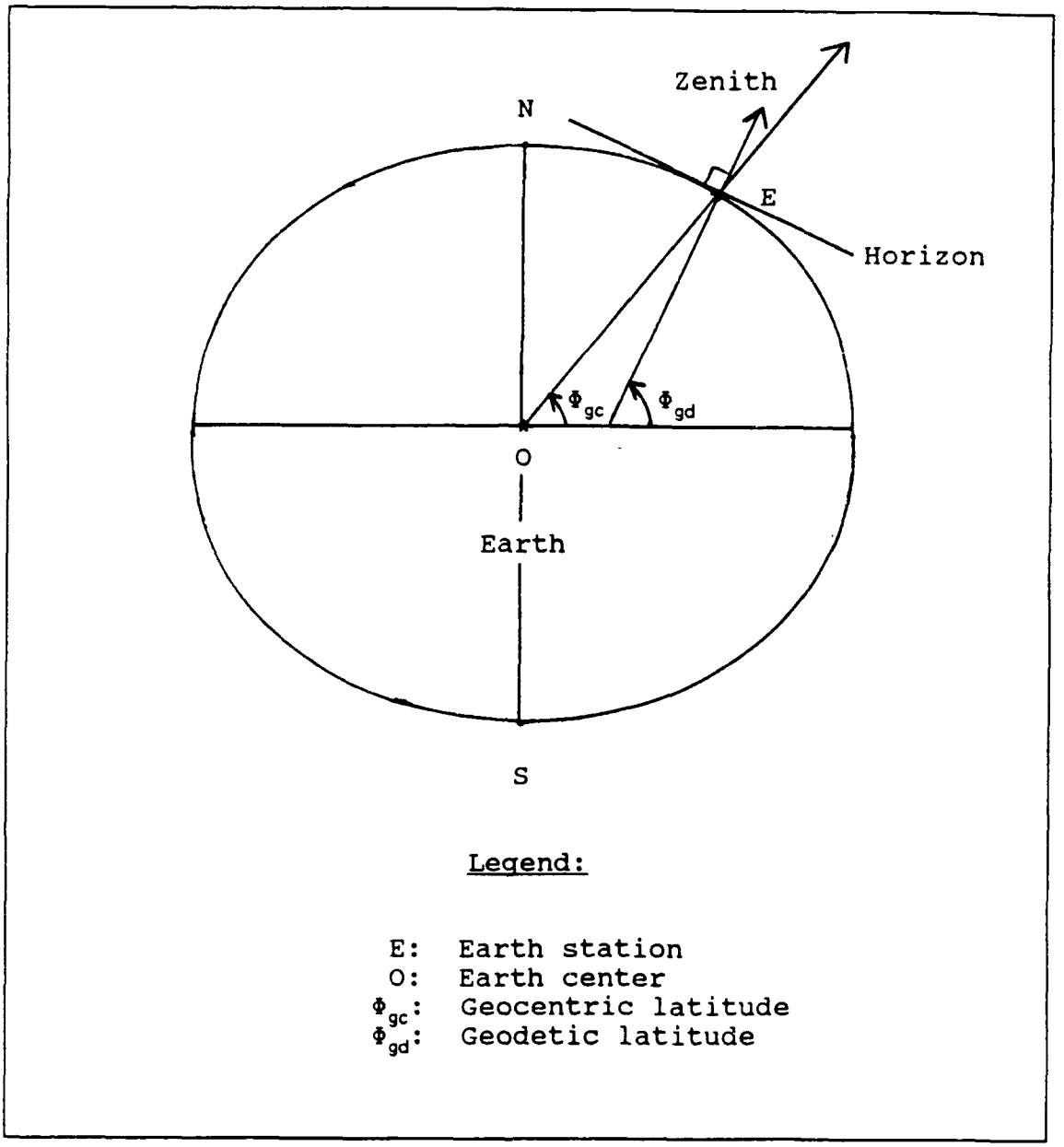

Figure 19. Geodetic vs. Geocentric Latitude

Direct Referencing

In direct referencing, line and pixel coordinates (l,p) are converted to geodetic coordinates (Φ_{gd}, λ_{gd}) for a given

pixel. Once the coordinates of each pixel are obtained, the data can be displayed using any projection method desired, resampling as required.

Assuming an oblate spheroid earth, a direct referencing algorithm is presented below.

STEP 0: Perform initial setup.

0.1 Calculate reference time t_0 for reference pixel (l_0, p_0) using mark time t at pixel coordinates (l,p) in Equation 47 (use HRPT pixel coordinates)

0.2 Calculate satellite position $\underline{r}$ and velocity $\underline{v}$ at reference time t_0 using a general elliptical orbit model

0.3 Calculate subpoint geocentric latitude Φ_{s_i} and longitude λ_{s_i} using Equations 50 - 52

0.4 If using spherical orbit approximation, calculate ascending node longitude λ_N and time t_N using Equations 34 - 38.

For each pixel with coordinates (l,p), do the following:

STEP 1: Calculate the pixel time and scan angle

1.1 If APT pixel coordinates, transform to HRPT pixel coordinates using Table 16

1.2 Calculate the pixel scan angle δ_p with Equation 46

1.3 Calculate the pixel time $t_{l,p}$ with Equation 47

STEP 2: Compute satellite position vector $\underline{r}$ and velocity vector $\underline{v}$ at time $t_{l,p}$

2.1 If using a general orbit, compute $\underline{r}$ and $\underline{v}$ using an elliptical orbit model

2.2 If using a local spherical orbit approximation, compute $\underline{r}$ and $\underline{v}$ using Equations 32 and 33

STEP 3: Compute or update scan direction $\hat{\underline{s}}$ as required using Equation 17

STEP 4: Compute range vector $\underline{d}$ from satellite to image point

4.1 Calculate range direction $\hat{\underline{d}}$ using Equation 18

4.2 Calculate range distance d using Equation 19 for a spherical earth, or using Equation 27 for an oblate spheroid earth.

4.3 Calculate range vector $\underline{d}$ with the identity $\underline{d} = d\hat{\underline{d}}$

STEP 5: Compute earth position vector $\underline{R}$ using Equation 16

STEP 6: Calculate geocentric latitude Φ_{gc} and longitude λ_{gc} using Equations 50 and 51

STEP 7: Convert to geodetic latitude Φ_{gd} and longitude λ_{gd} using Equations 53 and 54

Inverse Referencing

For inverse referencing, the object is to find the pixel that views a given earth location. This involves an iterative procedure of estimating the time of viewing, then making corrections for earth rotation to get progressively better time estimates.

Once the viewing time is known (with sufficient accuracy), the pixel coordinates in the image can be calculated. This can be used to overlay geographic outlines or grids on the satellite images.

The inverse referencing algorithm that follows applies to both elliptical orbits and spherical orbit approximations.

STEP 0: Perform initial setup.

0.1 Calculate reference time t_0 for reference pixel (l_0, p_0) using mark time t at pixel coordinates (l,p) in Equation 47 (use HRPT pixel coordinates)

0.2 If using a spherical orbit approximation, calculate satellite position $\underline{r}$ and velocity $\underline{v}$ at reference time t_0 using a general elliptical orbit model

For a given earth location E with geodetic coordinates $(\Phi_{gd}, \lambda_{gd})$, do the following:

STEP 1: Convert from geodetic coordinates to geocentric latitude Φ_{gc} and longitude λ_{gc} for earth location E, using Equations 53 and 54

STEP 2: Compute the equivalent time and longitude of the ascending node (equator crossing)

2.1 Calculate a reference subpoint position (ECI coordinates) at a reference time (say t_0) using a general elliptical orbit model

2.2 Calculate the geocentric latitude $\Phi_{S'}$ and longitude $\lambda_{S'}$ for subpoint S' with Equations 50 and 51

2.3 Use Equations 34-37 to calculate the time t_N and longitude λ_N of ascending node N

STEP 3: Guess a viewing time t_E (t_0 is good)

STEP 4: Estimate the scanning time of E, assuming no earth rotation

4.1 Compute the static longitude of E, λ'_E, using Equation 38

4.2 Compute related geometric measures β, j, and Ψ using Equations 39, 40, and 41, respectively

4.3 Using Equations 42 and 43, calculate the estimated scanning time $t_{S''}$ when the satellite reaches subpoint S"

STEP 5: Make an improved scan time guess, t', given by Equation 44

5.1 For better convergence, use convergence factor α computed using Equation 45

5.2 Using $\alpha = 1$ is easier, and nearly as good

STEP 6: Check the difference between $t_{S''}$ and t_E

6.1 If $|t_{S''} - t_E| < \epsilon$, go to STEP 7

6.2 If $|t_{S''} - t_E| > \epsilon$, return to STEP 4, substituting t' for t

STEP 7: Consider assumptions and accuracy desired

7.1 If local spherical orbit assumption is unsatisfactory, return to STEP 2, using an elliptical model to calculate the projected position of subpoint S'

7.2 If spherical earth approximation is unacceptable, compute earth location using direct referencing algorithm with an oblate spheroid earth, and compare to actual earth location to improve time estimate

7.3 Otherwise, proceed to STEP 8

STEP 8: Compute scan angle from Ψ using Equation 7

STEP 9: Compute pixel coordinates (l,p)

9.1 Calculate HRPT line number l and pixel number p using Equations 48 and 49, rounding to the closest integer

9.2 If using APT data, convert from HRPT to APT line and pixel numbers using Table 16

V. Conclusions/Recommendations

Conclusions

All the information necessary for the spatial registration of TIROS-N weather satellite images has been presented. The background theory has been explained and developed to meet registration requirements for both HRPT and APT data.

Specific registration algorithms were presented to convert pixel coordinates to geographic coordinates (direct referencing) and from geographic coordinates to pixel coordinates (inverse referencing). These algorithms are applicable for elliptical orbits, spherical orbits, or local spherical orbit approximations. The direct referencing algorithm allows the use of an oblate spheroid earth model, or a spherical earth model. The inverse referencing algorithm assumes a locally spherical earth, with guidelines for implementing an oblate spheroid earth model.

Preliminary testing using a personal computer verified the basic operation of the inverse referencing algorithm. A computer program applying the inverse referencing algorithm to overlay a map outline on a satellite image transmitted via APT is being written, though not completed as of this writing.

Recommendations

Having clearly set forth the means and use of spatial registration of TIROS-N weather satellite images, many useful applications and further improvements are possible. These include evaluating and improving the algorithm performance, calibration of the sensor data, and using the registered images for environmental (weather) analysis. Specific recommendations are:

1. Evaluate and improve registration algorithms
    a. Perform a complete validation and verification of the registration algorithms
    b. Evaluate algorithm performance using testing and sensitivity analysis
2. Develop associated computer programs to improve the use of registered images
    a. Analyze analog-to-digital conversion to get the best estimate of the original AVHRR words
    b. Develop a computer program to perform calibration of the sensor data
    c. Study various map projection techniques to display the satellite images
3. Use image registration for various applications using TIROS-N weather satellite data
    a. Design a geographic grid cell database for satellite data
    b. Perform time series analysis of registered satellite images
    c. Use satellite data for image identification and analysis (such as environmental and agricultural monitoring)

Bibliography

1. Barnes, James C. TIROS-N Series Direct Readout Services User's Guide. Washington: U.S. Department of Commerce, NOAA/NESDIS, March 1982.

2. Bate, Roger R. et al. Fundamentals of Astrodynamics. New York: Dover Publications, 1971.

3. Emery, William J. et al. "AVHRR Image Navigation: Summary and Review," Photogrammetric Engineering and Remote Sensing, 55: 1175-1183 (August 1989).

4. Haliday, David and Robert Resnick. Fundamentals of Physics. New York: John Wiley & Sons, 1974.

5. Hayes, L. and A.P. Cracknell. "A Comparison of TIROS-N Series Satellite Data and LANDSAT Data over Scotland," Proceedings of an EARsel/ESA Symposium on Integrative Approaches in Remote Sensing. 63-74. Noordwijk, The Netherlands: ESA Scientific and Technical Publications, 1984.

6. Ho, Diem and Adle Asem. "NOAA AVHRR Image Referencing," International Journal of Remote Sensing, 7: 895-904 (July 1986).

7. Kerr, Y. et al. "NOAA AVHRR Data as a Tool for Agricultural Monitoring," Proceedings of the 18th Symposium on Remote Sensing of Environments. 1041-1048. Ann Arbor: The Institute, 1984.

8. Kidwell, Catherine B. NOAA Polar Orbiter Data User's Guide. Washington: U.S. Department of Commerce, NOAA/-NESDIS, December 1986.

9. Ochiai, Hiroaki et al. "Joint Analysis of LANDSAT-MSS and NOAA-AVHRR Data for Marine Environmental Monitoring," Proceedings of the 13th International Symposium on Space Technology and Science. 1259-1264. Tokyo: AGNE Publishing Inc., 1982.

10. Planet, Walter G. Data Extraction and Calibration of TIROS-N/NOAA Radiometers. NOAA Technical Memorandum NESS 107-Rev. 1 Washington: U.S. Department of Commerce, NOAA/NESDIS, November 1979.

11. Popta, R.G. van. On-Line Superposition of Geographical Data to TIROS-N Type Meteorological Satellite Images. Amsterdam: National Aerospace Laboratory, 1982 (AD-B094 779).

12. Roy, A.E. and D. Clarke. Astronomy: Principles and Practice. New York: Crane Russak, 1977.

13. Schwalb, Arthur. Modified Version of the Tiros N/NOAA A-G Satellite Series (NOAA E-J) - Advanced Tiros N (ATN). NOAA Technical Memorandum NESS 116. Washington: U.S. Department of Commerce, NOAA/NESDIS, February 1982.

14. -----, Chief, Office of Systems Development. Telephone Interview. NOAA/NESDIS/OSD, Washington DC, 6 September 1989.

15. -----. The TIROS-N/NOAA A-G Satellite Series. NOAA Technical Memorandum NESS 95. Washington: U.S. Department of Commerce, NOAA/NESDIS, 1982.

16. Smith, Mona S. APT Information Note 89-2. Washington: U.S. Department of Commerce, NOAA/NESDIS, July 1989.

17. Summers, R. Joe. Educator's Guide for Building and Operating Environmental Satellite Receiving Stations. NOAA Technical Report NESDIS 44. Washington: U.S. Department of Commerce, NOAA/NESDIS, February 1989.

18. Sun, Weidong and Mikio Takagi. "Geometric Distortion Correction with High Accuracy for NOAA Satellite Images," Digest of the IEEE International Geoscience and Remote Sensing Symposium. 1257-1262. New York: IEEE Press, 1987.

19. Tozawa, Y. "Fast Geometric Correction of NOAA AVHRR," Proceedings of the IEEE 9th International Symposium on Machine Processing of Remotely Sensed Data. 46-53. New York: IEEE Press, 1983.

20. United States Naval Observatory. Astronomical Almanac for the Year 1988. Washington: Government Printing Office, 1987.

21. Wannamaker, Brian. "An Evaluation of Digitized APT Data from the TIROS-N/NOAA-A, -J Series of Meteorological Satellites," International Journal of Remote Sensing, 5: 133-144 (1984).

Vita

Captain Charles H. Larcomb [redacted] Graduating from the White Mountains Regional High School in Whitefield, New Hampshire, in 1976, he attended Bates College in Lewiston, Maine. He received the degree of Bachelor of Arts in Mathematics from Bates in June 1980. Upon completion of Officer Training School at Lackland AFB, Texas, he received his commission as an Air Force Officer on 1 July 1983. After a year of basic meteorology training at Saint Louis University, Missouri, he then served as a weather forecaster in the 2nd Weather Squadron at Barksdale AFB, Louisiana, supporting the 8th Air Force (SAC) until November 1985. An overseas tour followed at Howard AFB, Panama, where he met his wife, [redacted] He served as a weather officer in Detachment 25, 5th Weather Wing, supporting the U.S. Southern Command Headquarters, until entering the School of Engineering, Air Force Institute of Technology, in June 1988.

[redacted]

SECURITY CLASSIFICATION OF THIS PAGE

REPORT DOCUMENTATION PAGE

Form Approved
OMB No. 0704-0188

1a REPORT SECURITY CLASSIFICATION
UNCLASSIFIED

1b RESTRICTIVE MARKINGS

2a SECURITY CLASSIFICATION AUTHORITY

2b DECLASSIFICATION / DOWNGRADING SCHEDULE

3 DISTRIBUTION / AVAILABILITY OF REPORT
Approved for public release;
distribution unlimited

4 PERFORMING ORGANIZATION REPORT NUMBER(S)
AFIT/GSO/ENS/89D-10

5 MONITORING ORGANIZATION REPORT NUMBER(S)

6a NAME OF PERFORMING ORGANIZATION
School of Engineering

6b OFFICE SYMBOL (*If applicable*)
AFIT/ENS

7a NAME OF MONITORING ORGANIZATION

6c ADDRESS (*City, State, and ZIP Code*)
Air Force Institute of Technology
Wright-Patterson AFB OH 45433-6583

7b ADDRESS (*City, State, and ZIP Code*)

8a NAME OF FUNDING / SPONSORING ORGANIZATION

8b OFFICE SYMBOL (*If applicable*)

9 PROCUREMENT INSTRUMENT IDENTIFICATION NUMBER

8c ADDRESS (*City, State, and ZIP Code*)

10 SOURCE OF FUNDING NUMBERS

PROGRAM ELEMENT NO	PROJECT NO	TASK NO	WORK UNIT ACCESSION NO

11 TITLE (*Include Security Classification*)
SPATIAL REGISTRATION OF TIROS-N WEATHER SATELLITE DATA

12 PERSONAL AUTHOR(S)
Charles H. Larcomb, B.S., Captain, USAF

13a TYPE OF REPORT	13b TIME COVERED	14 DATE OF REPORT (*Year, Month, Day*)	15 PAGE COUNT
MS Thesis	FROM ____ TO ____	1989 December	95

16 SUPPLEMENTARY NOTATION

17 COSATI CODES			18 SUBJECT TERMS (*Continue on reverse if necessary and identify by block number*)
FIELD	GROUP	SUB-GROUP	
22	02		Image Registration — Space Sciences
08	02		Meteorological Satellites — Artificial Satellites

19 ABSTRACT (*Continue on reverse if necessary and identify by block number*)

Thesis Advisor: Thomas S. Kelso
Assistant Professor
Department of Operational Sciences

20 DISTRIBUTION / AVAILABILITY OF ABSTRACT	21 ABSTRACT SECURITY CLASSIFICATION
☒ UNCLASSIFIED/UNLIMITED ☐ SAME AS RPT ☐ DTIC USERS	UNCLASSIFIED

22a NAME OF RESPONSIBLE INDIVIDUAL	22b TELEPHONE (*Include Area Code*)	22c OFFICE SYMBOL
Thomas S. Kelso, Assistant Professor	(513) 255-3362	ENS

DD Form 1473, JUN 86 *Previous editions are obsolete*

The purpose of this study was to develop an algorithm to perform spatial registration of (assign geographic coordinates to) TIROS-N weather satellite data using a personal computer. Specific objectives were (1) to gather currently available information into a unified and understandable form, (2) to develop the background and related theory necessary for the registration of both High Resolution Picture Transmission (HRPT) and Automatic Picture Transmission (APT) data, and (3) to present a specific registration algorithm for TIROS-N weather satellite data.

The approach chosen is to use a general elliptical orbit model in conjunction with accurate satellite element sets (orbital parameters) to calculate accurate satellite positions at a given time. Knowing the earth movement and sensor operation as functions of time, the geographic locations of each pixel (picture element) are determined through geometric relations.

The algorithm presented converts pixel coordinates to, geographic coordinates (direct referencing) and vice versa (inverse referencing). These algorithms assume an elliptical orbit (with perturbations) and an oblate spheroid earth.

The most critical factor is found to be timing. A timing error of one second in computing satellite position produces an earth location error of about 6.5 kilometers at the satellite subpoint. A timing correction method is outlined to visually improve the image registration.